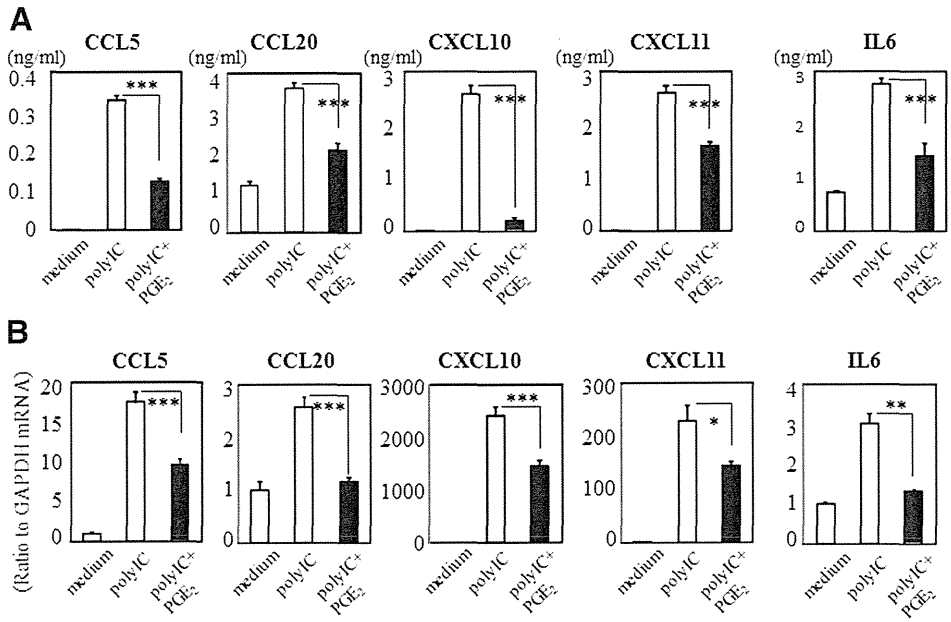

FIGURE 1. A, Suppression of the production of CCL5, CCl20, CXCL10, CXCL11, and IL-6 by PGE_2. HCLE were exposed to 10 μg/mL poly I:C and 100 μg/mL PGE_2 for 24 hours. Data are representative of 3 separate experiments and are given as the mean ± SEM from one experiment carried out in 6 wells per group. B, Suppression of mRNA expression of CCL5, CCL20, CXCL10, CXCL11, and IL-6 by PGE_2. HCLE were exposed to 10 μg/mL poly I:C and 100 μg/mL PGE_2 for 6 hours. The quantification data were normalized to the expression of the housekeeping gene *GAPDH*. The *y* axis shows the increase in specific mRNA over unstimulated samples. Data are representative of 3 separate experiments and are given as the mean ± SEM from one experiment carried out in 6 wells per group ($*P < 0.05$, $**P < 0.005$, $***P < 0.0005$).

lengths were obtained for EP2 (683 bp), EP3 (622 bp), and EP4 (956 bp) (Fig. 2), but not for EP1 (723 bp) (data not shown), from HCLE and *in vivo* human corneal epithelial cells, suggesting that the human corneal epithelium expresses EP2, EP3, and EP4 mRNAs. To confirm the specificity for the detection of EP2-, EP3-, and EP4 mRNA, we isolated and sequenced the PCR products. The obtained sequences were identical to the human EP2-, EP3-, and EP4 cDNA sequences. Moreover, we could detect EP2, EP3 and EP4 proteins using immunoblotting (see **Figure, Supplemental Digital Content 1**, http://links.lww.com/ICO/A42).

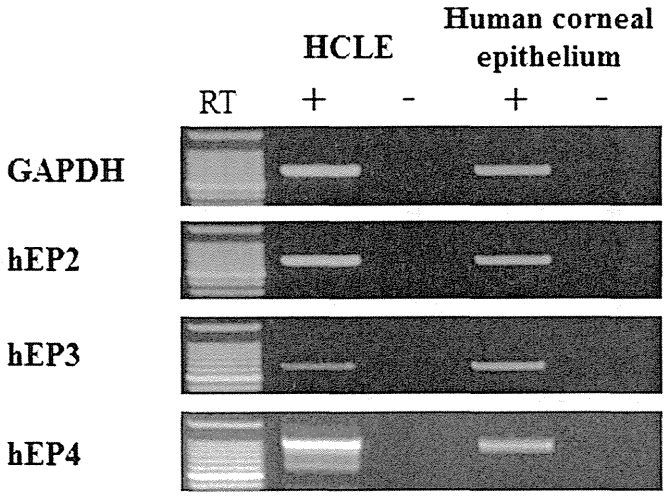

FIGURE 2. mRNA expression of the PGE_2 receptors EP2, EP3, and EP4. RT-PCR assay of the expression of PGE_2 receptor EP2, EP3, and EP4-specific mRNA in HLCE and human corneal epithelium. RT identifies data that were obtained without reverse transcription (controls).

EP2 and EP3, but not EP4 Agonists Downregulated the Production of Cytokines Induced by Poly I:C Stimulation

Using the EP2, EP3, and EP4 agonists, ONO-AE-259, ONO-AE-248, and ONO-AE-329, respectively, we also examined which PGE_2 receptor(s) contributed to their polyI:C-induced downregulation. HCLE were exposed to 10 μg/mL polyI:C and 10 μg/mL of the EP2, EP3, or EP4 agonist for 24 hours (ELISA) or 6 hours (quantitative RT-PCR). ELISA showed that the EP2 agonist significantly suppressed the polyI:C-induced production of CCL5, CXCL10, and CXCL11 (all, $P < 0.0005$) but not of CCL20 and IL-6, and that the EP3 agonist significantly suppressed the production of CCL5, CCL20, CXCL10, CXCL11, and IL-6 (all, $P < 0.0005$). However, the EP4 agonist failed to suppress the cytokine production induced by polyI:C stimulation (Fig. 3). Quantitative RT-PCR confirmed that the EP2 agonist significantly downregulated the mRNA expression of CCL5, CXCL10, and CXCL11 (respectively, $P < 0.005$, $P < 0.0005$ and $P < 0.05$), but not of CCL20 and IL-6, and that the EP3 agonist significantly downregulated the mRNA expression of all examined cytokines (CCL5, $P < 0.05$; CCL20, $P < 0.005$; CXCL10, $P < 0.0005$; CXCL11, $P < 0.0005$; and IL-6, $P <$ 0,005) (Fig. 4). Thus, our results show that PGE_2 attenuated the mRNA expression and production of CCL5, CXCL10, and CXCL11 via both EP2 and EP3, and that the CCL20 and IL-6 mRNA expression and production were attenuated only by EP3 in human corneal epithelial cells.

DISCUSSION

Lipid mediators like PGE_2 regulate immune and inflammatory responses by modulating the production of cytokines and chemokines.[11] In macrophages, PGE_2 suppressed the proinflammatory gene expression induced by LPS,

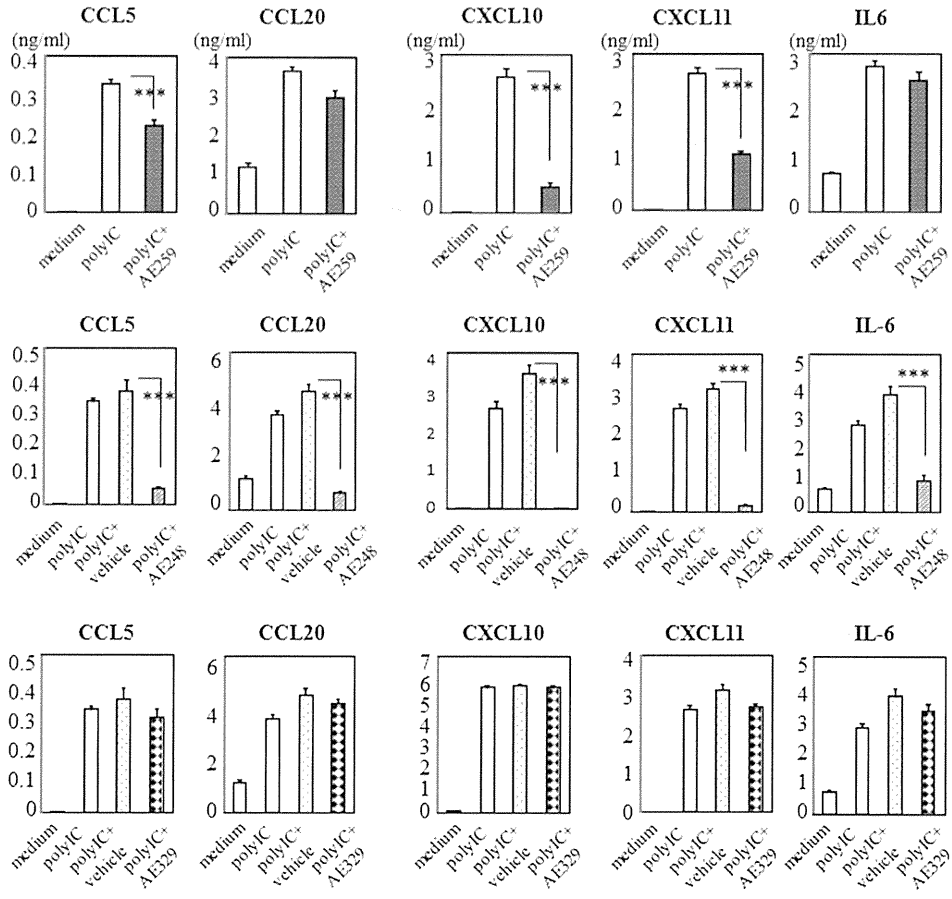

FIGURE 3. Effect of the PGE_2 receptors EP2, EP3, and EP4 on poly I:C-induced cytokine production. HCLE were exposed to 10 μg/mL poly I:C and 10 μg/mL EP2, EP3, or EP4 agonist for 24 hours. Data are representative of 3 separate experiments and are given as the mean ± SEM from one experiment carried out in 6 wells per group (***$P < 0.0005$).

including macrophage inflammatory protein (MIP)-1α, MIP-1β, CCL5, CXCL10, and IL-8.[9] Here we document that PGE_2 modulates the expression and production of polyI:C-induced proinflammatory genes in not only human conjunctival epithelial cells but also corneal epithelial cells. It exerted an inhibitory effect on polyI:C-induced CCL5, CCL20, CXCL10, CXCL11, and IL-6 mRNAs (respectively, $P < 0.0005$, $P < 0.0005$, $P < 0.0005$, $P < 0.05$ and $P < 0.005$) and on protein production in HCLE (all, $P < 0.0005$). PGE_2 exerts its biological actions by binding to EP located primarily on the plasma membrane. We confirmed the presence of the PGE_2 receptor subtypes, EP2,

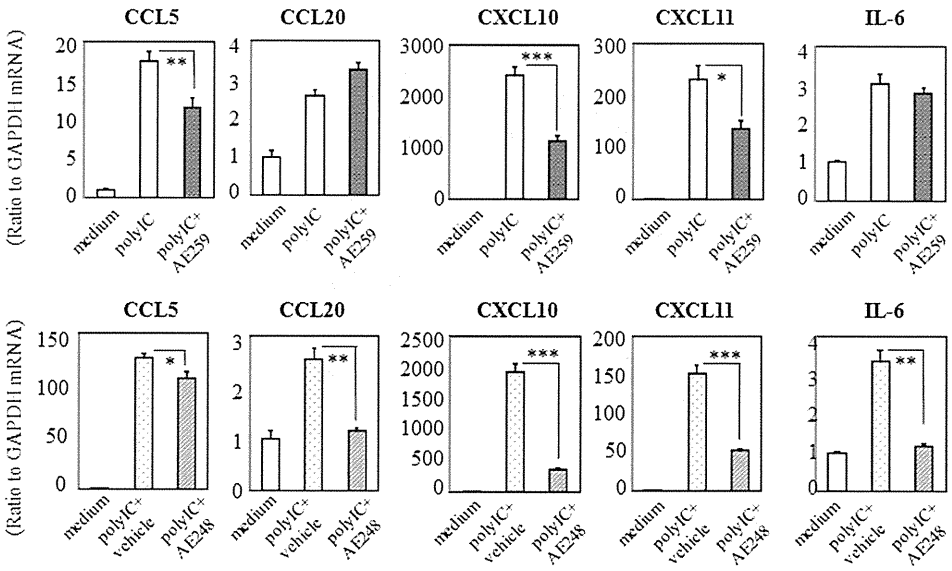

FIGURE 4. Effect of the PGE_2 receptors EP2 and EP3 on the poly I:C-induced mRNA expression of cytokines: HCLE were exposed to 10 μg/mL poly I:C and 10 μg/mL EP2 or EP3 agonist for 6 hours. The quantification data were normalized to the expression of the housekeeping gene *GAPDH*. The *y* axis shows the increase in specific mRNA over unstimulated samples. Data are representative of 3 separate experiments and are given as the mean ± SEM from one experiment carried out in 6 wells per group (*$P < 0.05$, **$P < 0.005$, ***$P < 0.0005$).

EP3, and EP4, in human corneal epithelial cells. Stimulation with either EP2- or EP3-specific agonists had a suppressive effect on polyI:C-induced CCL5, CXCL10, and CXCL11 production (both EP2- and EP3-specific agonists: all, $P < 0.0005$) , but only the EP3-specific agonist had a suppressive effect on the production of CCL20 and IL-6 (both, $P < 0.0005$).

Stimulation with PGE_2 exhibits immunosuppressive effects in various cell types including macrophages and dendritic cells via EP2 and/or EP4.[9–11] This phenomenon is explicable by the elevation of intracellular cyclic adenosine monophosphate (cAMP) via the activation of adenylcyclase.[9,10] Although PGE_2 acts on EP2 and EP4 and activates adenylcyclase, resulting in the elevation of intracellular cAMP, its action on EP3 suppresses adenylcyclase, resulting in a decrease in intracellular cAMP. In human conjunctival and corneal epithelial cells, both EP2 and EP3 contribute to the immunosuppressive effect against polyI:C stimulation; therefore, the suppressive effect cannot be explained by the elevation of intracellular cAMP. The precise molecular mechanisms underlying the immunosuppressive effects of PGE_2 in epithelial cells remain to be elucidated.

Release of PGE_2 is associated with ocular inflammation, but the exact role in inflammation has not been identified, rather PGE_2 might have been considered as inflammation-related molecules in the cornea. In this study, it is evident that PGE_2 could contribute to suppressing the production of various cytokines and chemokines in the ocular surface. Elsewhere we reported that PGE_2 acts as a ligand for EP3 in conjunctival epithelial cells and that it downregulates the progression of murine experimental allergic conjunctivitis,[7] suggesting the possibility of the PGE_2 and EP3 selective agonists as antiinflammatory drugs.

In summary, our results suggest that PGE_2 and its receptors in ocular surface (conjunctival and corneal) epithelium contribute to the regulation of ocular surface inflammation.

ACKNOWLEDGEMENTS

We thank Chikako Endo for technical assistance.

REFERENCES

1. Matsuoka T, Narumiya S. Prostaglandin receptor signaling in disease. *ScientificWorldJournal*. 2007;7:1329–1347.
2. Alexopoulou L, Holt AC, Medzhitov R, et al. Recognition of double-stranded RNA and activation of NF-kappaB by Toll-like receptor 3. *Nature*. 2001;413:732–738.
3. Ueta M, Kinoshita S. Ocular surface inflammation mediated by innate immunity. *Eye Contact Lens*. 2010;36:269–281.
4. Ueta M, Mizushima K, Yokoi N, et al. Gene-expression analysis of polyI:C-stimulated primary human conjunctival epithelial cells. *Br J Ophthalmol*. 2010;94:1528–1532.
5. Kumar A, Zhang J, Yu FS. Toll-like receptor 3 agonist poly(I:C)-induced antiviral response in human corneal epithelial cells. *Immunology*. 2006; 117:11–21.
6. Ueta M, Kawai T, Yokoi N, et al. Contribution of IPS-1 to polyI:C-induced cytokine production in conjunctival epithelial cells. *Biochem Biophys Res Commun*. 2011;404:419–423.
7. Ueta M, Matsuoka T, Narumiya S, et al. Prostaglandin E receptor subtype EP3 in conjunctival epithelium regulates late-phase reaction of experimental allergic conjunctivitis. *J Allergy Clin Immunol*. 2009;123:466–471.
8. Ueta M, Matsuoka T, Yokoi N, et al. Prostaglandin E2 suppresses polyinosine-polycytidylic acid (polyI:C)-stimulated cytokine production via prostaglandin E2 receptor (EP) 2 and 3 in human conjunctival epithelial cells. *Br J Ophthalmol*. 2011;95:859–863.
9. Takayama K, García-Cardena G, Sukhova GK, et al. Prostaglandin E2 suppresses chemokine production in human macrophages through the EP4 receptor. *J Biol Chem*. 2002;277:44147–44154.
10. Xu XJ, Reichner JS, Mastrofrancesco B, et al. Prostaglandin E2 suppresses lipopolysaccharide-stimulated IFN-beta production. *J Immunol*. 2008;180:2125–2131.
11. Shiraishi H, Yoshida H, Saeki K, et al. Prostaglandin E2 is a major soluble factor produced by stromal cells for preventing inflammatory cytokine production from dendritic cells. *Int Immunol*. 2008;20:1219–1229.
12. Ueta M, Hamuro J, Kiyono H, et al. Triggering of TLR3 by polyI:C in human corneal epithelial cells to induce inflammatory cytokines. *Biochem Biophys Res Commun*. 2005;331:285–294.
13. Ueta M, Kinoshita S. Innate immunity of the ocular surface. *Brain Res Bull*. 2010;81:219–228.
14. Ueta M, Sotozono C, Nakano M, et al. Association between prostaglandin E receptor 3 polymorphisms and Stevens-Johnson syndrome identified by means of a genome-wide association study. *J Allergy Clin Immunol*. 2010;126:1218–1225. e10.

CHOROIDAL THICKNESS IN INFERIOR STAPHYLOMA ASSOCIATED WITH POSTERIOR SEROUS RETINAL DETACHMENT

TETSUYA YAMAGISHI, MD, HIDEKI KOIZUMI, MD, PhD, TAIZO YAMAZAKI, MD, SHIGERU KINOSHITA, MD, PhD

Purpose: The purpose of the study was to describe the choroidal findings in eyes with posterior serous retinal detachment associated with inferior staphyloma by enhanced depth imaging optical coherence tomography.

Methods: The study involved five eyes of five patients with the inferior staphyloma accompanied by posterior serous retinal detachment. In each case, the upper border of the staphyloma was lying across the macula. Enhanced depth imaging spectral domain optical coherence tomography was performed in a vertical–sectional manner through the fovea, and the choroidal thicknesses at the thinnest point, at the fovea, and at 0.5 mm and 1.0 mm superior and inferior to the thinnest point were measured. Fluorescein angiography and indocyanine green angiography were also performed.

Results: In all 5 eyes, the choroid was thinnest at the upper border of the staphyloma (mean, 37.4 μm; SD, 13.5 μm; range, 23–53 μm). Fluorescein angiography showed a band of window defects along the upper border of the staphyloma, where indocyanine green angiography demonstrated persistent hypoperfusion in all 5 eyes.

Conclusion: The choroid was markedly thin at the upper border of the inferior staphyloma accompanied by posterior serous retinal detachment. Such choroidal abnormality seemed to play an important role in the development of serous retinal detachment.

RETINA 32:1237–1242, 2012

Tilted disk syndrome is a congenital anomaly associated with malclosure of the embryonic optic fissure. Typical findings are inferonasal tilting of the disk, peripapillary crescent, myopia, staphyloma of the affected inferonasal region, thinning of retinal pigment epithelium (RPE) in the inferonasal fundus, or visual field defect.[1] These findings were often seen in bilateral eyes. In addition, some eyes without tilted disk also have inferior staphyloma and associated with chorioretinal change or degeneration.

In eyes with inferior staphyloma, macular complications such as choroidal neovascularization,[2] polypoidal choroidal vasculopathy,[3] or serous retinal detachment (SRD)[4–6] occasionally develop and impair the visual function when the upper border of the inferior staphyloma traverses the macula. However, the pathogenesis of these complications still remains unknown. Especially, SRD of this kind rarely shows spontaneous resolution. Although some previous studies have reported performing laser photocoagulation, this disorder turned out to be refractory to the laser treatment or, even if once resolved, sometimes showed postoperative redetachment.[4,6] About the pathogenesis, there may be some difference between SRD with inferior staphyloma and central serous chorioretinopathy (CSC), which is one of the most typical causes for posterior SRD.

Spaide et al[7] recently reported the enhanced depth imaging optical coherence tomography (EDI-OCT) method to acquire cross-sectional images of the

From the Department of Ophthalmology, Kyoto Prefectural University of Medicine, Kyoto, Japan.

Supported in part by Grant No. 21890226 from Ministry of Education, Culture, Sports, Science and Technology, Japan (Dr. H. Koizumi).

The authors declare no conflict of interest.

Reprint requests: Hideki Koizumi, MD, PhD, 465 Kajii-cho, Kamigyo-ku, Kyoto 602–0841, Japan; e-mail: hidekoiz@koto.kpu-m.ac.jp

choroid using a conventional spectral domain optical coherence tomography. This method improves the visualization of the intrachoroidal structure and chorioscleral interface. Using EDI-OCT, the choroidal thickness also can be measured.[8–11]

In this report, we performed EDI-OCT on eyes with posterior SRD associated with the inferior staphyloma for the purpose of providing new insights into the pathogenesis.

Patients and Methods

Retrospective analyses were performed on consecutive patients with SRD related to the inferior staphyloma. All patients underwent comprehensive ocular examinations including refractive error measurement, visual acuity testing using Landolt C charts, indirect slit-lamp biomicroscopy, color fundus photography, fluorescein angiography (FA), indocyanine green angiography (ICGA), and spectral domain optical coherence tomography.

Eyes with foveal SRD associated with the inferior staphyloma lying across the macula were included. Eyes were excluded if they had a history of previous intravitreal injection of any medication, a history of intraocular surgery or laser procedure (conventional laser photocoagulation, photodynamic therapy, or transpupillary thermotherapy), CSC, any type of choroidal neovascularization, any retinal vascular abnormalities, or use of any systemic or ocular corticosteroids. The EDI-OCT procedure was reported previously.[7] Briefly, the choroid was imaged by positioning the spectral domain optical coherence tomography (3D-OCT 1000 Mark II; Topcon Corp, Tokyo, Japan) device close enough to the eye to obtain an inverted image that automatically appears on the monitor to match those seen with conventional imaging. The 6-mm vertical scan, comprising a maximum of 16 averaged scans, was obtained through the center of the fovea of each eye. On this enhanced image, the choroidal thicknesses at the thinnest point around the macula, at the fovea, and at 0.5 mm and 1.0 mm superior and inferior to the thinnest point were measured perpendicularly to the RPE layers as the distance between the hyperreflective line corresponding to the outer surface of the RPE and the chorioscleral interface by use of the electronic caliper within the optical coherence tomography device. Fluorescein angiography and ICGA were performed with a confocal scanning laser ophthalmoscope (Heidelberg Retina Angiograph 2; Heidelberg Engineering, Dossenheim, Germany). Obtained images were correlated with the fundus photographs and the EDI-OCT images.

The choroidal thickness at each point was defined as the mean value of those measured by two independent observers. The paired *t*-test was used to evaluate the reproducibility of choroidal thickness measurement between the observers. Statistical analyses were performed using StatView software version 5.0 (SAS Institute, Inc, Cary, NC). A probability value of $P < 0.05$ was considered to be statistically significant.

The study protocol followed the tenets set forth in the Declaration of Helsinki, and ethics approval was obtained from the Institute Review Board of Kyoto Prefectural University of Medicine.

Results

There were five eyes of five patients diagnosed as having inferior staphyloma with SRD. All patients presented with visual loss and/or metamorphopsia. The mean age of the subjects was 50.2 years (SD, 21.5 years). Four of the five patients were women. The mean spherical equivalent was −3.4 diopters (SD, 2.0 diopters), and all eyes were phakic. Three of the five patients had bilateral tilted disk syndrome and bilateral inferior staphyloma; however, they had unilateral SRD. The other two eyes had unilateral inferior staphyloma and SRD without tilted disk syndrome.

The representative cases are shown in Figures 1 and 2. All five eyes biomicroscopically showed depigmentation of the RPE along the upper border of the staphyloma and SRD involving the center of the fovea. On the EDI-OCT images, the cross-sectional images of the choroid were visualized. In each of the five eyes, the upper border of the staphyloma traversed the macula and was located inferiorly to the foveal center. At the site of the upper border of the staphyloma, there was a finding of a markedly thin choroid. The average value of the choroidal thickness was 37.4 μm (SD, 13.4 μm; range, 23–53 μm) at the thinnest point around the macula and was 172.1 μm (SD, 44.7 μm; range, 110–219 μm) at the fovea. The characteristics and choroidal thicknesses of each case are summarized in Table 1. The choroidal thicknesses independently measured by the 2 observers were not significantly different ($P = 0.78$). The choroid became thicker superiorly and inferiorly to the thinnest point (Figure 3). On FA, a band of window defects were seen in all five eyes at the site of the RPE depigmentation observed under biomicroscopic examination. In three of the five eyes, FA demonstrated one or more focal active leaking sites inside the areas of the window defects. In the other two eyes, FA demonstrated no visible leaking sites. On the ICGA of all five eyes, an evident hypofluorescent band was

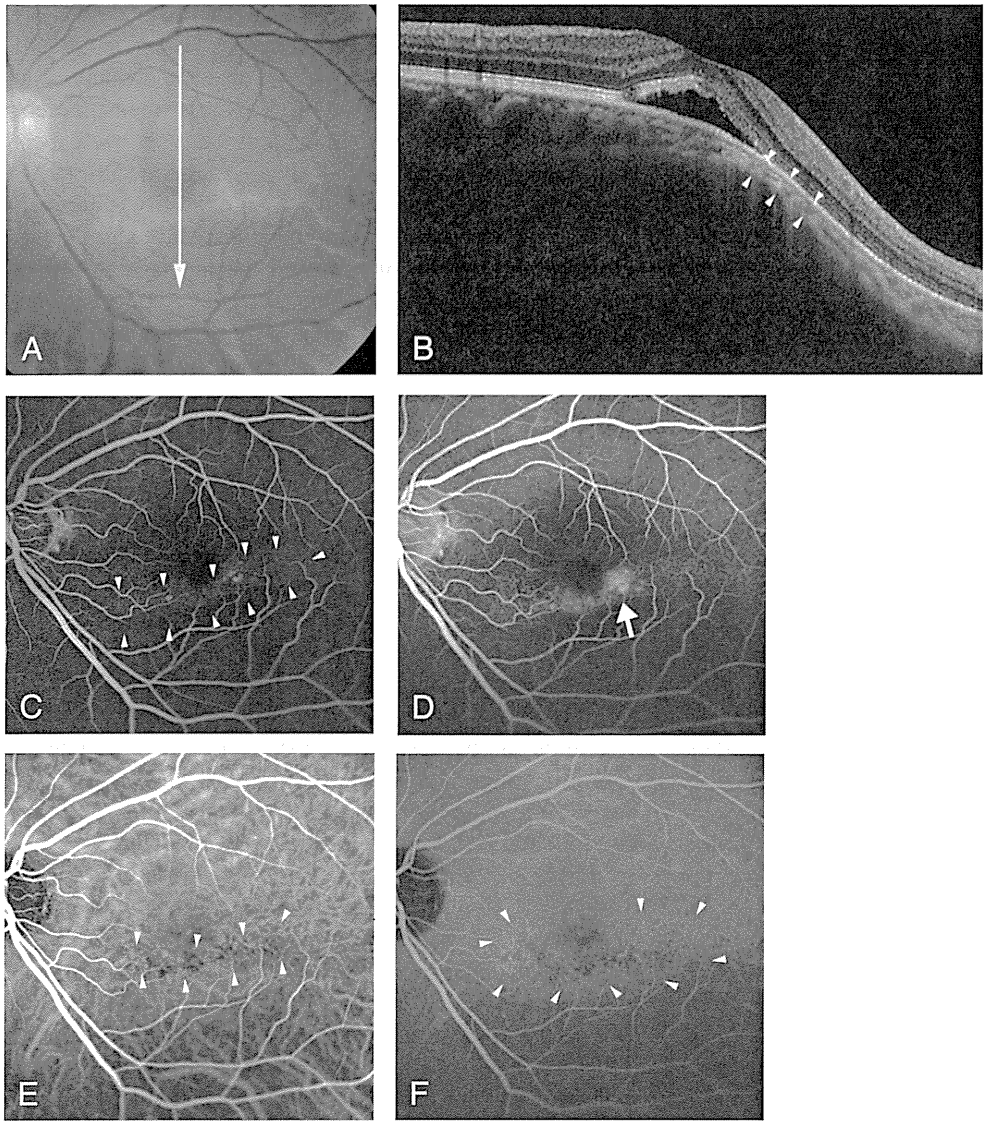

Fig. 1. Case 1. A 45-year-old woman with foveal retinal detachment associated with inferior staphyloma. The best-corrected visual acuity was 0.6 (decimal). **A,** Color fundus photograph of the left eye shows inferior staphyloma and foveal retinal detachment. Note that the upper border of the staphyloma lies across the macula. The arrow corresponds to a section examined with EDI-OCT. **B,** The vertical–sectional image through the fovea obtained with EDI-OCT displays subfoveal fluid and the markedly thin choroid (arrowheads) at the upper border of the staphyloma. The choroidal thickness at the thinnest point was 53 μm. **C,** The mid phase of FA demonstrates a band of window defects (arrowheads) corresponding to the upper border of the staphyloma. **D,** The late phase of FA reveals a focal leaking point in the parafoveal area (white arrow). **E,** The early phase of ICGA shows a hypofluorescent band (arrowheads). **F,** The late phase of ICGA demonstrates subtle hyperfluorescence (arrowheads) around the hypofluorescent band seen in the early phase.

detected corresponding to the areas of RPE depigmentation in the early phase and it was surrounded by subtle hyperfluorescence in the late phase.

Discussion

The findings of this study demonstrated marked thinning of the choroid at the upper border of the staphyloma associated with posterior SRD. The choroid appeared to be thicker superiorly and inferiorly to the thinnest point. This unique choroidal abnormality might have a relationship with the development of the SRD.

The upper border of the inferior staphyloma often traverses the macula. Cohen and Quentel[15] suggested that in eyes with tilted disk syndrome, the progression of the staphyloma may express upward traction on the RPE, the Bruch membrane, and the choriocapillaris complex from the upper border of the staphyloma. Although speculative, the upward traction superior to this border might possibly be related to anatomical changes of RPE (RPE atrophy) and choroid (choroidal thinning).

In the present study, EDI-OCT revealed a very thin choroid of 37.4 μm on average at the upper border of the staphyloma. By means of EDI-OCT, it was reported that the subfoveal choroidal thickness was 287 μm in healthy eyes[9] and 93.2 μm in highly myopic eyes.[8] Accordingly, in our cases, the choroidal thickness at the upper border of staphyloma was much less than that at the fovea in healthy eyes and even less than that in highly myopic eyes.

Although several reports have been published about this disorder, the detail of the pathogenesis

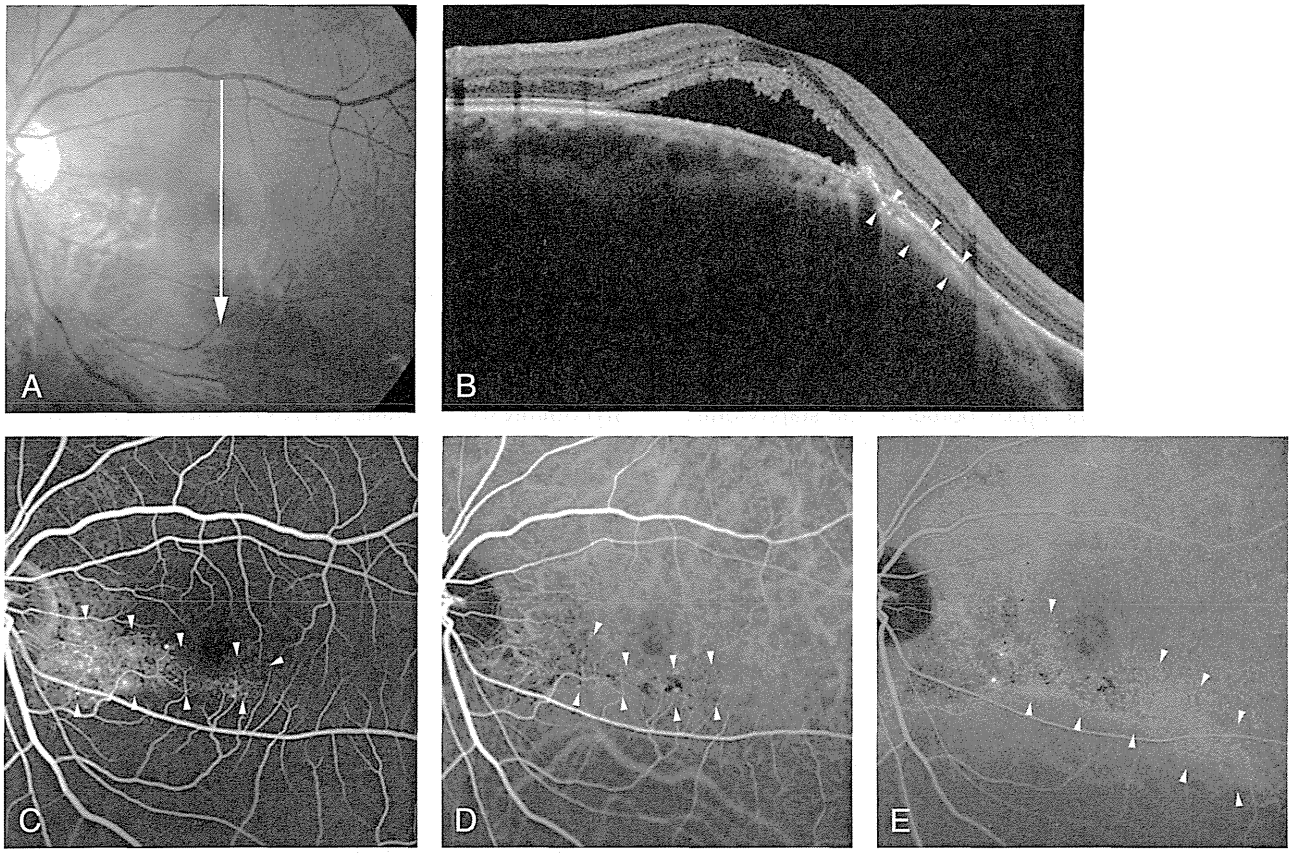

Fig. 2. Case 3. A 44-year-old woman with foveal retinal detachment associated with inferior staphyloma. The best-corrected visual acuity was 1.2 (decimal). **A,** Color fundus photograph of the left eye shows inferior staphyloma with SRD involving the fovea. The upper border of the staphyloma traversed the macula. The arrow indicates a section examined with EDI-OCT. **B,** The vertical–sectional image through the fovea obtained with EDI-OCT demonstrates subretinal fluid and a markedly thin choroid (arrowheads) at the upper border of the staphyloma. The choroidal thickness at the thinnest point was 23 μm. **C,** The mid phase of FA shows a band of window defects (arrowheads) along the upper border of the staphyloma. This case showed no active leakage in all phases of FA. **D,** The early phase of ICGA demonstrated hypofluorescent band (arrowheads). **E,** The late phase of ICGA showed subtle hyperfluorescence (arrowheads) around the hypofluorescent band seen in the early phase.

remains unclear. Cohen et al[4] and later Leys and Cohen[6] described FA findings in tilted disk syndrome with posterior SRD and mentioned that not only RPE dysfunction but also anomalies of the choroidal perfusion at the upper border of the staphyloma could explain the SRD. This theory could be supported by an experimental study by Yao and Marmor[16] who demonstrated that in rabbit eyes, RPE damage alone was not sufficient to cause SRD; however, both RPE and the choriocapillaris should be impaired to induce SRD. In the same study, it was also proved that SRD spontaneously resolved when the choriocapillaris was not damaged, even in the absence of RPE. Therefore, the choroid appeared to play a key role in the accumulation and resorption of SRD rather than RPE. There is a direction of flow from the vitreous to the choroid, and the latter acts as a means of fluid resorption. All five cases in the present study showed both RPE atrophy and a very thin choroid at the upper border of the inferior staphyloma. The decreased ability of the choroid to remove the SRD may be responsible, at least in part, for the development of posterior SRD.

Nakanishi et al[17] reported the pathophysiology of tilted disk syndrome with macular complications including SRD. In their study, the hypofluorescent area was seen at the upper border of the staphyloma in the early phase of ICGA, later surrounded by hyperfluorescence seen in the late phase. They hypothesized that the hyperfluorescence might indicate choroidal vascular hyperpermeability, which was also previously reported to be seen in eyes with CSC,[12–14] probably induced by a possible mechanical force or hemodynamic change. The choroid in eyes with CSC was markedly thick compared with that of normal eyes.[11] Our cases also revealed ICGA findings similar to those shown by Nakanishi et al, but the EDI-OCT images obtained in our study demonstrated apparent thinning

Table 1. Characteristics and Choroidal Thicknesses of the Patients with Foveal SRD Associated with Inferior Staphyloma

Case	Gender	Eye	Age (Years)	BCVA (Decimal)	Spherical Equivalent (D)	Choroidal Thickness at the Thinnest Point (μm)	Subfoveal Choroidal Thickness (μm)
1	F	L	45	0.6	−2.0	53	166
2	F	R	25	1.0	−5.0	46	219
3	F	L	44	1.2	−1.5	23	212
4	M	L	84	0.3	−2.5	42	110
5	F	L	53	1.0	−6.0	25	155
Mean choroidal thickness						37.4 ± 13.4 (SD)	172.1 ± 44.7 (SD)

BCVA, best-corrected visual acuity; D, diopters; F, female; L, left eye; M, male; R, right eye.

of the choroid at the upper border of the staphyloma. Thus, we believe that the pathogenesis of SRD seen in our cases might be somewhat different from that of CSC.

The present study had several limitations. The number of cases was limited. The images of the EDI-OCT were obtained in a single line, and the choroidal thickness measurement did not cover the overall macular area. Although the use of EDI-OCT allowed for the subfoveal choroidal thickness to be evaluated with a lesser number of images than previously reported,[7] the optical coherence tomography used in this study did not include the eye tracking system and thus may present a weakness in obtaining images with the best contrast. This study was only a cross-sectional study, and the follow-up period was limited. Thus, further studies are required to elucidate the pathogenesis of the disorder.

In conclusion, the findings of the study showed the marked thinning of the choroid at the upper border of the staphyloma in eyes with posterior SRD associated with inferior staphyloma. At the same lesion, the hypofluorescent finding on ICGA was evident. Both the RPE dysfunctions and the choroidal circulatory disturbances might possibly be attributed to the pathogenesis of SRD.

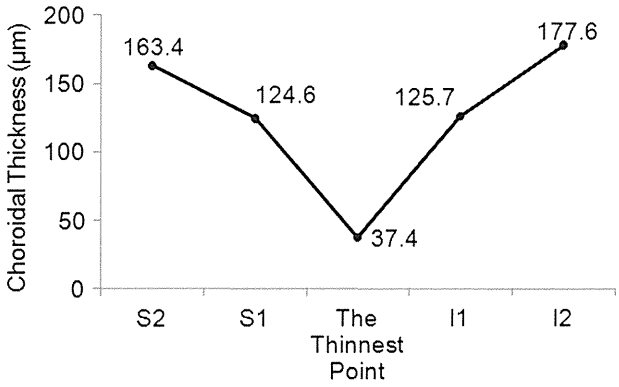

Fig. 3. The average values of the choroidal thicknesses at and around the thinnest point. The choroid was relatively thick at the superior and inferior sites compared with the thinnest point; S1, 0.5 mm superior; S2, 1.0 mm superior; I1, 0.5 mm inferior; I2, 1.0 mm inferior to the thinnest point. The numbers adjacent to the plotted points shown in the graph represent the averaged choroidal thicknesses at each point.

Key words: tilted disk syndrome, inferior staphyloma, serous retinal detachment, optical coherence tomography, enhanced depth imaging optical coherence tomography (EDI-OCT), choroid, choroidal thickness, retinal pigment epithelium.

References

1. Apple DJ, Rabb MF, Walsh PM. Congenital anomalies of the optic disc. Surv Ophthalmol 1982;27:3–41.
2. Tsuboi S, Uchihori Y, Manabe R. Subretinal neovascularisation in eyes with localised inferior posterior staphyloma. Br J Ophthalmol 1984;68:869–872.
3. Mauget-Faysse M, Cornut PL, Quaranta El-Maftouhi M, Leys A. Polypoidal choroidal vasculopathy in tilted disk syndrome and high myopia with staphyloma. Am J Ophthalmol 2006;142:970–975.
4. Cohen SY, Quentel G, Guiberteau B, et al. Macular serous retinal detachment caused by subretinal leakage in tilted disc syndrome. Ophthalmology 1998;105:1831–1834.
5. Tosti G. Serous macular detachment and tilted disc syndrome. Ophthalmology 1999;106:1453–1455.
6. Leys AM, Cohen SY. Subretinal leakage in myopic eyes with a posterior staphyloma or tilted disk syndrome. Retina 2002; 22:659–665.
7. Spaide RF, Koizumi H, Pozzoni MC. Enhanced depth imaging spectral-domain optical coherence tomography. Am J Ophthalmol 2008;146:496–500.
8. Fujiwara T, Imamura Y, Margolis R, et al. Enhanced depth imaging optical coherence tomography of the choroid in highly myopic eyes. Am J Ophthalmol 2009;148:445–450.
9. Margolis R, Spaide RF. A pilot study of enhanced depth imaging optical coherence tomography of the choroid in normal eyes. Am J Ophthalmol 2009;147:811–815.
10. Spaide RF. Enhanced depth imaging optical coherence tomography of retinal pigment epithelial detachment in age-related macular degeneration. Am J Ophthalmol 2009; 147:644–652.
11. Imamura Y, Fujiwara T, Margolis R, Spaide RF. Enhanced depth imaging optical coherence tomography of the choroid in central serous chorioretinopathy. Retina 2009;29: 1469–1473.

12. Giovannini A, Scassellati-Sforzolini B, D'Altobrando E, et al. Choroidal findings in the course of idiopathic serous pigment epithelium detachment detected by indocyanine green videoangiography. Retina 1997;17:286–293.
13. Iida T, Kishi S, Hagimura N, Shimizu K. Persistent and bilateral choroidal vascular abnormalities in central serous chorioretinopathy. Retina 1999;19:508–512.
14. Prunte C, Flammer J. Choroidal capillary and venous congestion in central serous chorioretinopathy. Am J Ophthalmol 1996;121:26–34.
15. Cohen SY, Quentel G. Chorioretinal folds as a consequence of inferior staphyloma associated with tilted disc syndrome. Graefes Arch Clin Exp Ophthalmol 2006;244:1536–1538.
16. Yao XY, Marmor MF. Induction of serous retinal detachment in rabbit eyes by pigment epithelial and choriocapillary injury. Arch Ophthalmol 1992;110:541–546.
17. Nakanishi H, Tsujikawa A, Gotoh N, et al. Macular complications on the border of an inferior staphyloma associated with tilted disc syndrome. Retina 2008;28:1493–1501.

Common Variants in *CDKN2B-AS1* Associated with Optic-Nerve Vulnerability of Glaucoma Identified by Genome-Wide Association Studies in Japanese

Masakazu Nakano[1☯], Yoko Ikeda[2☯], Yuichi Tokuda[1☯], Masahiro Fuwa[1,3], Natsue Omi[1], Morio Ueno[2], Kojiro Imai[2], Hiroko Adachi[1], Masaaki Kageyama[3], Kazuhiko Mori[2], Shigeru Kinoshita[2]*, Kei Tashiro[1]*

1 Department of Genomic Medical Sciences, Kyoto Prefectural University of Medicine, Kyoto, Japan, **2** Department of Ophthalmology, Kyoto Prefectural University of Medicine, Kyoto, Japan, **3** Research and Development Center, Santen Pharmaceutical Co. Ltd., Nara, Japan

Abstract

Background: To date, only a small portion of the genetic variation for primary open-angle glaucoma (POAG), the major type of glaucoma, has been elucidated.

Methods and Principal Findings: We examined our two data sets of the genome-wide association studies (GWAS) derived from a total of 2,219 Japanese subjects. First, we performed a GWAS by analyzing 653,519 autosomal common single-nucleotide polymorphisms (SNPs) in 833 POAG patients and 686 controls. As a result, five variants that passed the Bonferroni correction were identified in *CDKN2B-AS1* on chromosome 9p21.3, which was already reported to be a significant locus in the Caucasian population. Moreover, we combined the data set with our previous GWAS data set derived from 411 POAG patients and 289 controls by the Mantel-Haenszel test, and all of the combined variants showed stronger association with POAG ($P<5.8\times10^{-10}$). We then subdivided the case groups into two subtypes based on the value of intraocular pressure (IOP)—POAG with high IOP (high pressure glaucoma, HPG) and that with normal IOP (normal pressure glaucoma, NPG)—and performed the GWAS using the two data sets, as the prevalence of NPG in Japanese is much higher than in Caucasians. The results suggested that the variants from the same *CDKN2B-AS1* locus were likely to be significant for NPG patients.

Conclusions and Significance: In this study, we successfully identified POAG-associated variants in the *CDKN2B-AS1* locus using a Japanese population, i.e., variants originally reported as being associated with the Caucasian population. Although we cannot rule out that the significance could be due to the differences in sample size between HPG and NPG, the variants could be associated specifically with the vulnerability of the optic nerve to IOP, which is useful for investigating the etiology of glaucoma.

Citation: Nakano M, Ikeda Y, Tokuda Y, Fuwa M, Omi N, et al. (2012) Common Variants in *CDKN2B-AS1* Associated with Optic-Nerve Vulnerability of Glaucoma Identified by Genome-Wide Association Studies in Japanese. PLoS ONE 7(3): e33389. doi:10.1371/journal.pone.0033389

Editor: John R. B. Perry, Peninsula College of Medicine and Dentistry, United Kingdom

Received September 1, 2011; **Accepted** February 13, 2012; **Published** March 12, 2012

Funding: This work was supported by the grants from the Collaborative Development of Innovative Seeds of Japan Science and Technology Agency (JST) to MK and KT, from the Ministry of Health, Labor and Welfare of Japan to KM, SK and KT, and from Santen Pharmaceutical Co. Ltd. to SK and KT. The funders had no role in study design, data collection and analysis, decision to publish, or preparation of the manuscript.

Competing Interests: This study has been completed under the Collaborative Research Agreement executed by Kyoto Prefectural University of Medicine and Santen Pharmaceutical Co., Ltd. All materials and information produced throughout this study are parts of co-owned intellectual properties. MF and MK are employees of Santen Pharmaceutical Co., Ltd. This does not alter the authors' adherence to all the PLoS ONE policies on sharing data and materials.

* E-mail: tashiro@koto.kpu-m.ac.jp (KT); shigeruk@koto.kpu-m.ac.jp (SK)

☯ These authors contributed equally to this work.

Introduction

Glaucoma is a neurodegenerative ocular disease and one of the leading causes of irreversible blindness worldwide [1]. It is characterized by the progressive loss of retinal ganglion cells and optic nerve axons, resulting in visual field defects [2]. One of the well-known major risk factors for glaucoma is elevated intraocular pressure (IOP) [2]. Thus, the measurement of IOP is routinely involved in the diagnosis of glaucoma. In fact, the IOP level has been applied to subdivide the most common form of glaucoma, primary open-angle glaucoma (POAG), into two subtypes [3]: POAG with high (≥22 mmHg) IOP (POAG/HPG, high pressure glaucoma; hereafter referred to as "HPG") and with normal (<22 mmHg) IOP (POAG/NPG, normal pressure glaucoma; hereafter referred to as "NPG"). Interestingly, ~92% of the Japanese POAG patients are categorized into the NPG subtype [4], whereas ~41% of Caucasian POAG patients are categorized as NPG [5], thus showing a unique epidemiological distribution of Japanese patients compared with other ethnic groups.

Aside from IOP measurements, the diagnosis of glaucoma is commonly made by observing optic nerve degeneration and visual field defects by means of fundus examinations and visual field tests, respectively. In the case of HPG, early drug treatment to lower IOP immediately following the onset of visual field damage has been shown to be quite effective in slowing the irreversible progression toward blindness [6,7]. In contrast, since NPG

patients show normal IOP, they are often misdiagnosed. Therefore, both fundus examinations of the optic nerve and visual field tests are critical for the proper diagnosis of NPG patients. However, due to the restriction of the healthcare expenditure to include those examinations into a person's regular medical checkup, especially in the preclinical state of glaucoma, it would be of great benefit if the risk of developing glaucoma could be ascertained based on a simple blood test to assess the genetic markers for the disease.

Since glaucoma shows familial aggregation and its prevalence varies between individuals of different ethnicities, it has been theorized that genetic factors play a significant role in the pathogenesis of glaucoma [8,9]. Therefore, several institutions are making profound efforts to discover single-nucleotide variants for glaucoma by conducting a genome-wide association study (GWAS) [10–14], and there are a few published reports of the association of particular loci, such as the *CAV1/CAV2* locus (7q31.1) [13] and the *TMCO1* or *CDKN2B-AS1* loci (1q24.1 or 9p21.3, respectively) [14], with POAG using Caucasian subjects. However, it appears that a controversy still exists as to determining the authentic variants associating with POAG, even within the same ethnicity of European descent [14,15]. We previously reported a GWAS and the subsequent follow-up study focused on the high-ranked variants identified in the initial population using in total of 1,575 Japanese subjects [10]. We identified six variants located in three loci, 1q43, 10p12.31, and 12q21.31, on the chromosome which were modestly associated with POAG, although the association results were not reproducible with a different population of different ethnicities [13,16,17]. In that previous study, we combined the patients from both HPG and NPG subtypes as a single case group in order to increase the statistical power [10]. Therefore, the genetic loci that were identified are most likely to be components of the molecular mechanism shared by both subtypes. Another Japanese group performed a GWAS [12] and discovered variants in *SRBD1* on 2p21 and *ELOVL5* on 6p12.1 that were associated with NPG (in that study, NPG was referred to as "normal tension glaucoma") [18]. However, since the findings in that study were derived from a single population, replication studies to support those findings still need to be conducted.

In this present study, we examined two independent GWAS data sets, and then performed a meta-analysis by combining the data sets in order to discover authentic genetic markers for POAG, HPG, or NPG. We succeeded in identifying some significant variants in the *CDKN2B-AS1* locus using a Japanese population, as that locus has also been shown to be significantly associated with POAG in Caucasians [14]. Moreover, the variants that passed the Bonferroni correction seemed to be associated with POAG and POAG/NPG, thus suggesting that the locus potentially affects the NPG, rather than the HPG, subtype of POAG. Although we still need to confirm our findings by use of a larger HPG cohort in order to increase the statistical power, the variants identified in this study could be associated specifically with the vulnerability of the optic nerve to IOP, thus enabling us to investigate the etiology of glaucoma.

Results

We first performed a GWAS in 833 POAG patients and 686 control subjects (hereafter referred to as "Present GWAS"; Figure 1A) who were selected and divided into case and control groups based on our strict diagnosis criteria. After genotyping, 653,519 SNPs passed the quality controls and were used for the association study (Figure 1A). In a quantile-quantile (Q-Q) plot

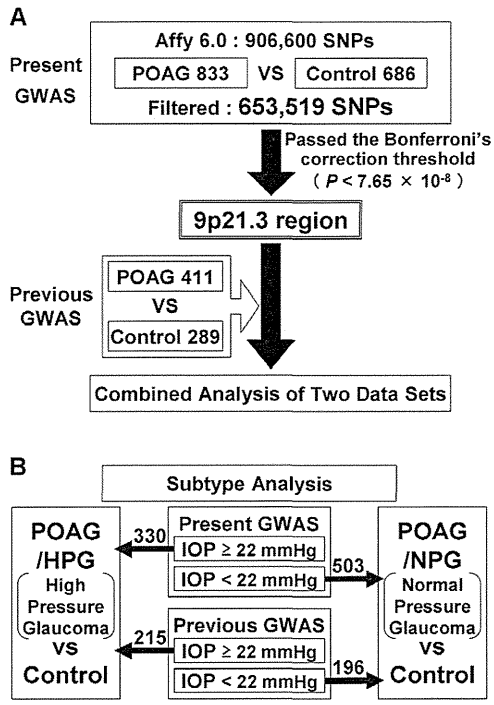

Figure 1. Study design. (A) We first performed the "Present GWAS" for POAG and identified the 9p21.3 locus. This result was confirmed by the combined analysis with the "Previous GWAS". (B) We then subdivided the POAG subjects into two subtypes, POAG/HPG and POAG/NPG, and each group was analyzed by combining the two data sets in order to investigate the differences of statistical significance in the 9p21.3 locus.
doi:10.1371/journal.pone.0033389.g001

(Figure S1A), the genomic inflation factor (λ) showed 1.021, suggesting that the population substructure should not have any substantial effects on the association analysis. Under these conditions, we obtained 8 genome-wide significant SNPs (Table S1) that passed the Bonferroni correction threshold ($0.05/653{,}519 = 7.65\times10^{-8}$), of which 5 SNPs were located in *CDKN2B-AS1* on chromosome 9p21.3 (Figure 2). A few SNPs that showed modest to strong association were distributed across a single linkage disequilibrium (LD) block located in the locus (Figure S2). The remaining genome-wide significant SNPs identified from different chromosomes turned out to be genotyping errors due to the poor 2D clusters (Figure S3B–D).

Next, we updated the case and control groups of the previous GWAS population [10] with the latest clinical information and ended up with 411 POAG patients and 289 controls (hereafter referred to as "Previous GWAS"; Figure 1A). One SNP (rs8181047) of 5 genome-wide significant SNPs in *CDKN2B-AS1* identified from the Present GWAS was not able to be assessed in the Previous GWAS because a DNA probe of that particular SNP was not designed for the Affymetrix 500 K platform. Consequently, we combined the two sets of GWAS genotype data for the remaining 4 SNPs by use of the Mantel-Haenszel test [19], and the level of significance of all 4 SNPs increased from $P<5.2\times10^{-9}$ to $P<5.8\times10^{-10}$ (Table 1). These 4 SNPs were highly correlated with one another ($r^2>0.98$), and were considered to have a similar effect for POAG based on the conditional analysis. These results suggested that it was effective to combine the data since the population stratification between the two data sets seemed to be ignorable, which was also supported by the results of the heterogeneity test. Moreover, we assessed the confounding effects

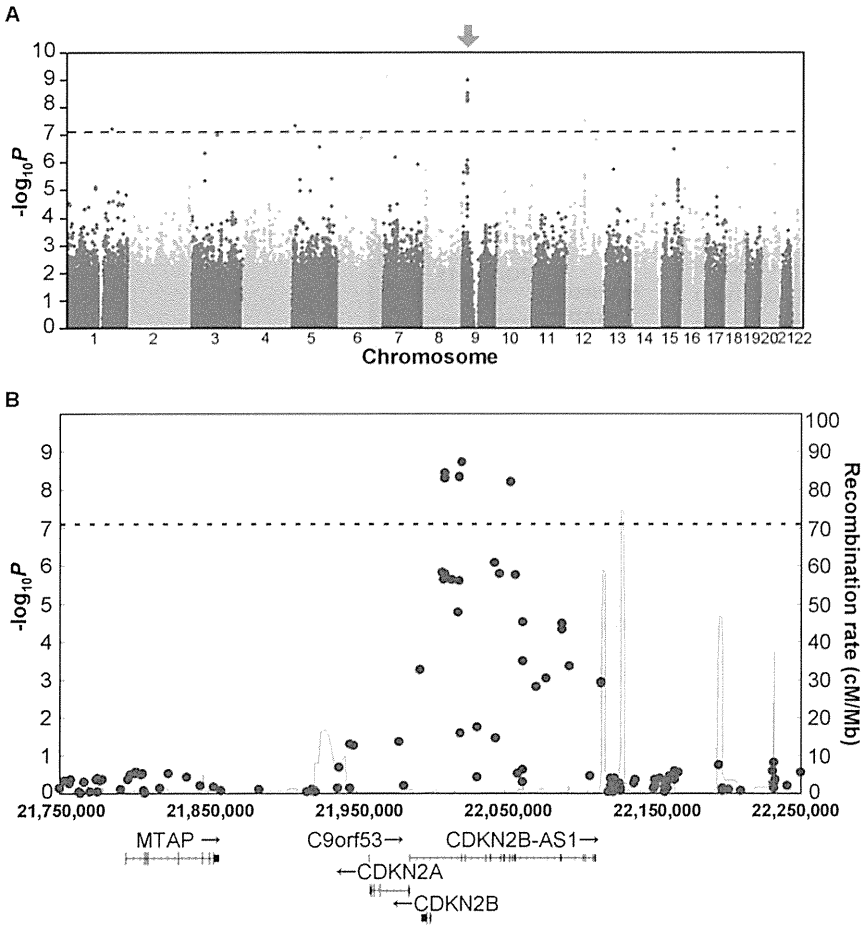

Figure 2. Association results of the Present GWAS. (A) The SNPs with a strong association appeared to exist in a cluster on chromosome 9 (red arrow). (B) The five significant SNPs that passed the Bonferroni correction threshold (horizontal dotted line) were identified in *CDKN2B-AS1* on the 9p21 locus. SNP positions followed the NCBI Build 36 coordinates. The genetic recombination rates (cM/Mb) estimated by HapMap Project [31] in Release 22 are indicated by the thin blue line.
doi:10.1371/journal.pone.0033389.g002

for these SNPs with respect to age and gender, and none were found to be statistically significant (Table S2), thus suggesting that the obtained association results were specific to the case-control comparison. In addition, the two sets of GWAS data for 40 SNPs surrounding the significant 4 SNPs in the 9p21.3 locus were also combined and analyzed (Table S3, Table S4). Since these 44 SNPs, in total, were genotyped in both the Present and Previous GWAS, and all of the SNPs passed the genotyping quality controls, these SNPs should prove useful in providing a broader overview of the significance of the locus. The results showed that the significance of combined SNPs was generally high between 22.0–22.1 Mb (Figure 3A). Within the particular locus, there seemed to be two distinct LD blocks; one in the side including genome-wide significant SNPs ("LD Block 1" in Figure 3D) and one in the other side with modestly associated SNPs ("LD Block 2" in Figure 3D).

Table 1. Association results of genome-wide significant SNPs in the Present GWAS.

			Previous GWAS			Present GWAS			Previous & Present Combined		
SNP:risk allele	**Chr.**	**Position**	**Frequency[a]**	***P***	**OR (95% CI)**	**Frequency[a]**	***P***	**OR (95% CI)**	***P*[b]**	**OR (95% CI)**	**Het-*P*[c]**
rs523096:A	9	22,009,129	0.89/0.84	6.0×10^{-3}	1.56 (1.13–2.14)	0.89/0.82	3.8×10^{-9}	1.86 (1.51–2.29)	1.6×10^{-10}	1.76 (1.48–2.10)	0.42
rs518394:C	9	22,009,673	0.89/0.85	1.5×10^{-2}	1.49 (1.08–2.07)	0.89/0.82	5.2×10^{-9}	1.85 (1.50–2.28)	5.8×10^{-10}	1.74 (1.46–2.07)	0.34
rs564398:A	9	22,019,547	0.90/0.85	4.7×10^{-3}	1.58 (1.15–2.18)	0.90/0.82	4.6×10^{-9}	1.86 (1.51–2.29)	1.4×10^{-10}	1.77 (1.49–2.11)	0.47
rs7865618:A	9	22,021,005	0.90/0.85	6.3×10^{-3}	1.56 (1.13–2.14)	0.90/0.82	2.0×10^{-9}	1.88 (1.53–2.32)	9.0×10^{-11}	1.78 (1.50–2.12)	0.39

[a]Risk allele frequency in POAG/controls.
[b]*P* value of combined 2 GWAS results by Mantel-Haenszel test.
[c]*P* value of Cochran's Q heterogeneity test between Previous and Present GWAS.
doi:10.1371/journal.pone.0033389.t001

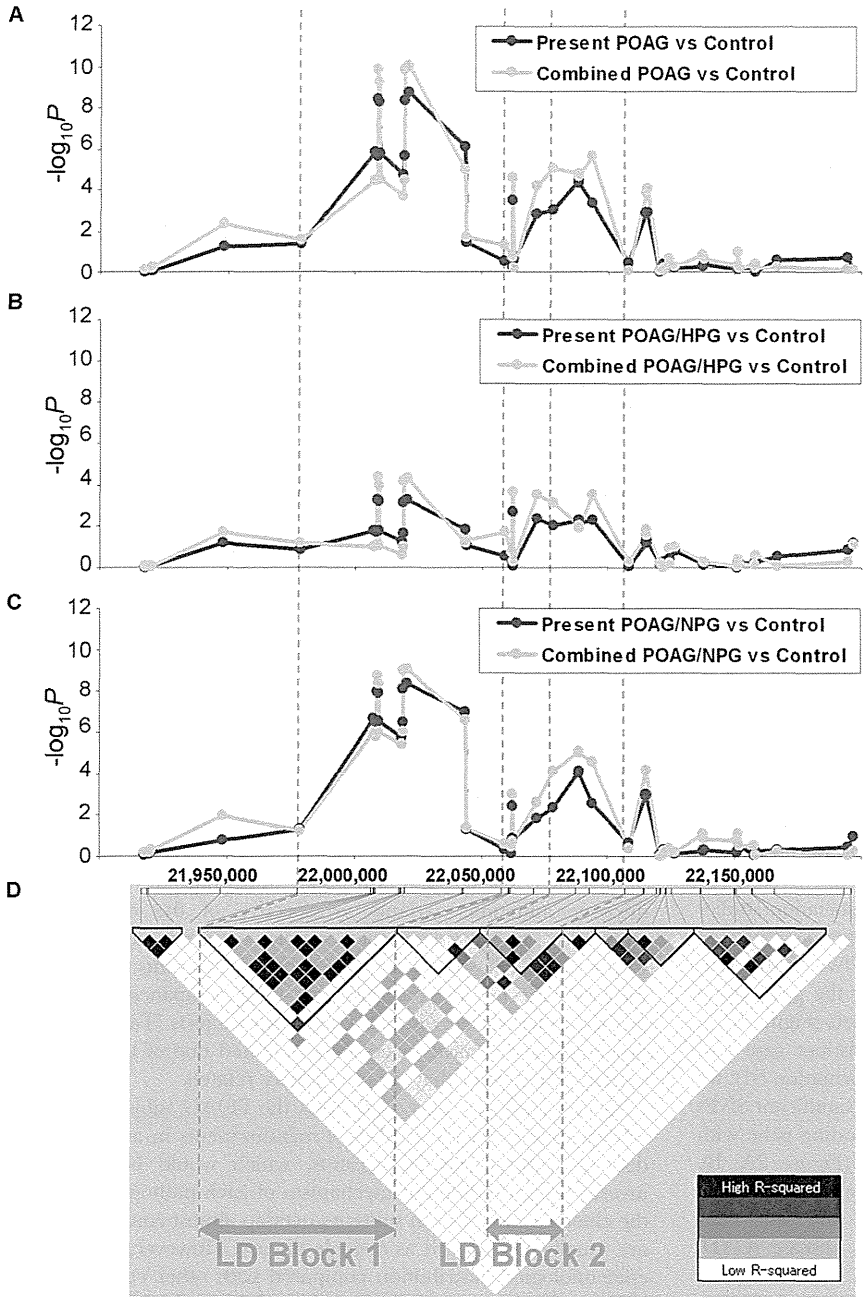

Figure 3. Combined analysis of the Present and Previous GWAS data in 9p21.3 locus. Three graphs representing the results of the association studies for POAG (A), HPG (B), and NPG (C) are shown in order from upper to lower, respectively. The results derived from the Present GWAS alone or the two combined GWAS data sets are indicated by the purple or green line graph plots, respectively. The lowest plot (D) shows an LD plot in the same region. All of the Present and Previous GWAS subject data was applied to draw the LD plot by Haploview v4.2. The color indicating pairwise r^2 and LD block were lined by using the confidence interval (95%) of pairwise D'. Vertical dashed redline indicates the same region between the upper graphs and LD Block 1 and 2 at the lowest.
doi:10.1371/journal.pone.0033389.g003

For the subtype analyses (Figure 1B), the POAG patients from both the Present and Previous GWAS populations were divided into two subtypes based on the clinical record of IOP measurement: 1) POAG patients with HPG (IOP≥22 mmHg) and 2) those with NPG (i.e., patients who consistently showed an IOP of less than 22 mmHg) [3]. The number of subjects in each subtype was found to be 330 HPG and 503 NPG patients and 215 HPG and 196 NPG patients in the Present and Previous GWAS, respectively (Figure 1B). When we performed the analysis separately using the Present GWAS data set, the Q-Q plots of HPG vs control and NPG vs control appeared to be quite different from one another (Figure S1B, C). In particular, the HPG results indicated non-deviated Q-Q plots (Figure S1B). In fact, although none of the SNPs were genome-wide significant for HPG (Figure S4A), we obtained 4 genome-wide significant SNPs that passed the Bonferroni correction threshold for NPG (Table S1, Figure S4B). As for NPG, the significance level of all 4 SNPs also increased when the two data sets were combined (Figure 3C, Table S3,

Table S4), however, the significance was still far from the Bonferroni threshold of significance in relation to HPG (Figure 3B, Table S3, Table S4). Although the significance level of SNPs residing in LD Block 2 showed slight differences among the different subtypes, the level in LD Block 1 seemed to be determining the difference of significance between the two subtypes, thus suggesting that the variants on LD Block 1 are closely associated with the susceptibility to glaucoma in the 9p21.3 locus (Figure 3D). Surprisingly, all of the significant SNPs from NPG overlapped with those obtained from POAG (Table S1). However, when we performed the heterogeneity test between the HPG and NPG groups, the results were not significant ($P = 0.21$–0.25, Table S3), suggesting that the significant differences between the two subtypes could be due to the small sample size of the HPG group. Although we need to confirm the above results using a larger HPG cohort, these results suggested that the significant SNPs identified in *CDKN2B-AS1* on the 9p21.3 locus probably serve as genetic markers of glaucoma, which could be useful for investigating the etiology of glaucoma with respect to the vulnerability of the optic nerve to IOP.

Discussion

In this study, we successfully identified genetic markers in *CDKN2B-AS1* strongly associated with POAG and POAG/NPG, but not with HPG, by analyzing two GWAS data sets using independent study populations totaling 2,219 Japanese subjects. For the case-control study of the Present GWAS, we excluded the samples without hesitation that didn't meet our strict quality control (see Supporting Information S1). Since we succeeded in excluding the samples possessing a fair amount of no-call or missed-call genotype data, our more stringent filters certainly improved the actual genotyping results for the association studies performed later. Thus, we were able to obtain an increased level of significance without any substructure effects of the two populations based on the definite diagnosis when combining the genotyping results of the Present and Previous GWAS data sets (Figure 3).

Using our polished data sets derived from distinct case and control subjects (see Methods and Supporting Information S1), we succeeded in identifying a cluster of genome-wide significant SNPs associated with POAG in *CDKN2B-AS1*, a non-coding gene with an unknown function, on chromosome 9p21.3 (Figure 2A, B). Several variants in chromosome 9p21 have been found to be associated with a variety of common diseases, and 9p21 was initially identified as a locus for coronary artery disease (CAD) [20–23] and type-2 diabetes [24–26]. However, little is known about the biological meanings underlying the locus, as 9p21 is a "gene desert" locus and most of the variants identified were non-coding. Recently, Harismendy et al. [27] reported that they have identified 33 enhancers in 9p21, some of which being within *CDKN2B-AS1*, and it turned out to be the second densest gene desert for predicted enhancers, thus suggesting the regulatory role of sequences residing within non-coding loci. They finally determined a few adjacent, as well as distant (>45 kb), target gene regions relevant to CAD biology physically interacting with the enhancer by 3D-DSL (also known as "4C"), a chromatin conformation capture technology, in human vascular endothelial cells. Overall, their study has provided an excellent example of a solution to link the unknown meanings of statistical association to a biological function. Since the POAG variants were also identified in *CDKN2B-AS1*, the variants would probably affect the expression level of the downstream genes *CDKN2A* and *CDKN2B*. In fact, Burdon et al. reported up-regulated *CDKN2A* and *CDKN2B* expression in response to the elevated IOP [14], suggesting the involvement of the locus in molecular pathways leading to glaucoma development. Moreover, the possibility that the variants would also affect the distant unidentified target genes in the context of the complex etiology of glaucoma, as well as the nature of the identified locus [27], cannot be ruled out.

To date, several institutions have attempted to discover variants for glaucoma by conducting a GWAS, and a few published studies have reported the association of particular loci with POAG using Caucasian subjects (Table S5). Thorleifsson et al. reported the association of common variants near *CAV1/CAV2* on 7q31.1 using a population of European ancestry [13]. In contrast, Kuehn et al. reported that they failed to replicate their results in a United States cohort [15]. Moreover, meta-analysis of the association results derived from several institutions of Northern Europe, including the data from Thorleifsson et al. [13], identified a few new loci associated with POAG, including the *CDKN2B-AS1* locus on 9p21.3 [17]. Recently, the new loci at *TMCO1* on 1q24.1 and *CDKN2B-AS1* were reported to be associated with Australian populations [14]. Thus far, only the association of the *CDKN2B-AS1* locus was replicated, even within the same ethnicity of European descent. Interestingly, Thorleifsson et al. also showed a modest association with the *CAV1/CAV2* locus using Chinese subjects [13], although the allele frequency of the particular variant in Asian subjects was quite low when compared with that in Caucasians, suggesting etiological differences due to the genetic background. In fact, according to the results of our Present GWAS for POAG, we were unable to replicate the association with the *CAV1/CAV2* and *TMCO1* loci (Figure S5F, G, Table S5). Moreover, in the Present GWAS, we were unable to replicate the association results of the 6 SNPs identified in the previous study [10] (Table S5), even though the populations were of the same ethnic background, thus suggesting that we still need to discover authentic variants, irrespective of the difference in ethnicities, to elucidate the complex etiology of glaucoma. Consequently, it should be noted that the variants identified in the *CDKN2B-AS1* locus in this study using a Japanese population seemed to be shared with the Caucasian subjects (Table S5), thus showing that we have successfully obtained one of the authentic variants for POAG that is not ethnicity related.

In this study, we also subdivided the POAG subjects into two subtypes based on the IOP level measurements in an attempt to discover subtype-specific variants, which would be useful for investigating the different mechanism of each pathogenesis. Since the clinical states of both subtypes overlap almost completely, they are usually categorized as a single disease. However, as a unique epidemiological distribution compared with other ethnic groups, ~92% of the Japanese POAG patients fall into the NPG category, as determined by the Tajimi study [4], a robust epidemiology study. In fact, another Japanese group performed a GWAS focused on discovering NPG-specific variants [12]. They reported that the SNPs in *SRBD1* on 7q31.1 and *ELOVL5* on 6p12.1 were associated with NPG, although our group was unable to replicate those results (Figure S5D, E). On the contrary, we obtained an unexpected result that the variants associated with NPG were completely identical to those associated with POAG in *CDKN2B-AS1* identified in this study (Table S1). In contrast, none of the variants were significant for HPG (Figure 3B). Although we cannot rule out that the significance could be due to the differences in sample size between HPG and NPG cases according to the heterogeneity test ($P = 0.21$–0.25; Table S3), the results suggested that the genetic loci identified are most likely components of the molecular mechanism specific for NPG. It has been reported that there are differences in vulnerability of the optic nerve to IOP between HPG and NPG [18]. It has also been theorized that

CDKN2B-AS1 affects the susceptibility of the optic nerve [14,28]. Since the variants identified in this study seemed to be shared among different ethnicities in functional aspects as well, the other variants should be contributing to the unique epidemiology of NPG in Japanese. By continuing to build upon the detailed investigation, such as obtaining in-depth sequencing data of the non-coding 9p21 locus, it might be possible to reveal not only the molecular mechanism of glaucoma pathogenesis but also the genetic diversity that resides within the locus among different ethnic backgrounds.

Methods

Ethics statement

This study was approved by the Institutional Review Board of Kyoto Prefectural University of Medicine and all procedures were conducted in accordance with the Declaration of Helsinki. All participants provided written informed consent after an explanation of the nature and possible consequences of the study.

Case and control subjects for the Present GWAS

All participants were interviewed to determine their familial history of glaucoma and other ocular or general diseases. A total of 2,126 Japanese participants, including POAG patients, healthy volunteers, and patients with other ocular diseases, were recruited between March 2005 and December 2010 at the University Hospital of Kyoto Prefectural University of Medicine (Kyoto, Japan) to give peripheral blood samples for this study. A third person who was blind to both the blood sampling and genotyping assigned an anonymous code to each blood sample. Genomic DNA used for the genotyping experiments was isolated from the blood, and Epstein-Barr virus (EBV)-transformed lymphocytes were prepared from the remaining blood as previously described [29] to serve as the future resource of genomic DNA. POAG patients and controls suitable for this study were precisely selected based on the strict diagnosis as previously described [10]. In particular, subtype selection was performed by dividing POAG into two categories according to peak IOP without treatment; POAG/High Pressure Glaucoma (POAG/HPG, defined as ≥22 mmHg) and POAG/Normal Pressure Glaucoma (POAG/NPG) [3]. All of the diagnostic procedures, including case-control selection and subtype classification, were performed by three ophthalmologists (YI, MU, and KM) from a single institution. The age and female/male ratio of all of the subjects used in the Present and Previous GWAS are shown in Table S6. To examine the possible confounding effects of age and gender, we assessed the correlations between the values and the genotype data from the case and control samples by one-way ANOVA or chi-square test (Table S2).

SNP genotyping and quality control for the Present GWAS

First, 906,600 SNPs were genotyped for 2,126 Japanese subjects by Genome-Wide Human SNP Array 6.0 (Affymetrix, Santa Clara, CA) according to the manufacturer's instructions. As for the Present GWAS population, 839 POAG patients and 708 controls were selected after performing the quality control (QC) as described (Supporting Information S1). To exclude the potential inclusion of genetically related subjects into the population, identity-by-descent (IBD) estimates were performed for all possible combinations by PLINK v1.07 (http://pngu.mgh.harvard.edu/~purcell/plink/). In total, 6 POAG patients and 22 controls were assumed to be in first-degree relationships or in relationships with a few more-distant relatives, and were thus excluded from the Present GWAS population. Finally, the Present GWAS population ended up with 833 POAG patients, comprised of 330 HPG and 503 NPG patients, and 686 controls. Population stratification for the present GWAS population was examined by principal component analysis using EIGENSTRAT software v3.0 (http://genepath.med.harvard.edu/~reich/Software.htm). As for the reference genomic population, the four HapMap populations (CEU, YRI, JPT, and CHB) were simultaneously applied to EIGENSTRAT. The generated cluster plots indicated that our POAG and control population was genetically clustered within the JPT population, and there was no outlier sample (Figure S6). We performed SNP quality control for the population on the autosomal SNPs based on the following QC filters: (i) call rate per SNPs in case and control samples ≥95%, (ii) minor allele frequency (MAF) in case and control samples ≥1%, and (iii) Hardy-Weinberg equilibrium (HWE) in control samples P≥0.001. Consequently, we analyzed the remaining 653,519 SNPs for the Present GWAS population.

Population update for reanalyzing the Previous GWAS

Since 6 years had passed since the patients and healthy volunteers who participated in our Previous GWAS [10] were first recruited, we updated the case (n = 418) and control (n = 300) groups based on the latest clinical information. In total, 7 samples from the case group and 11 samples from the healthy control group were removed. The population for the reanalysis finally ended up with 411 POAG patients, comprised of 215 HPG and 196 NPG patients, and 289 controls. The Previous GWAS data was obtained by GeneChip® Human Mapping 500 K Array platform (Affymetrix) containing 500,568 SNPs. The quality control for the reanalysis was performed by using the same QC filters as used in the Present GWAS. Genotype data derived from the particular locus for combining with the Present GWAS data was extracted from these filtered SNPs.

Data management and statistical analysis

To manage and analyze all of the genotype data, we used our in-house Genoika Server System (SASA Plus Co., Ltd., Fukuoka, Japan), which was well improved from the system used in the Previous GWAS [10,30] by the same system engineers. In addition, to manage the Previous GWAS data effectively, the Labo Server System (World Fusion Co., Ltd.) was used simultaneously. The Genoika Server System comes with PLINK v1.07 (http://pngu.mgh.harvard.edu/~purcell/plink/), the R program v 2.9.2 and 2.10.1 (http://www.r-project.org/), EIGENSTRAT software v3.0 (http://genepath.med.harvard.edu/~reich/Software.htm), and Haploview 4.2 (http://www.broadinstitute.org/scientific-community/science/programs/medical-and-population-genetics/haploview/haploview) built in, and all the analyses were performed by use of this system. In addition, Microsoft Office Excel 2003 (Microsoft Corporation, Redmond, WA) was used for preparing the data sets and statistical analysis. The frequency of alleles in the case and control samples was compared by use of the basic allele test. The odds ratio (OR) and the upper and lower limit of the 95% confidence interval (CI) of each SNP were calculated for the allele possessing a higher frequency in the case samples than in the control samples. The HWE was evaluated by the chi-square test. Q-Q plots were generated by ranking the observed values from minimum to maximum and plotting them against their expected chi-square values using the "snpMatrix" package ver 1.14.6 in the R program (http://www.r-project.org/). We applied the Mantel-Haenszel test [19] to combine the data derived from the two data sets in order to reduce potential negative effects arising from the

biases in age and female/male ratio among the populations (Table S6).

Supporting Information

Figure S1 Q-Q plots for the Present GWAS. Quantile-quantile (Q-Q) plots for the Present GWAS of POAG (A), HPG (B), and NPG (C) were generated by ranking the observed chi-square values from minimum to maximum and plotting them against their expected values. Genomic inflation factors (λ) are also shown. These plots were created using the R-package snpMatrix.
(PDF)

Figure S2 LD plots in the 9p21 locus. LD plots were generated from the Present GWAS data. The SNPs applied to these plots and the span of the region are the same as shown in Figure 2B. Upper and lower plots indicate the value of pairwise D′ and r2, respectively. The positions of 5 SNPs, which passed the Bonferroni correction threshold in the Present GWAS, are drawn in vertical dashed lines. These LD plots were generated using Haploview v4.2.
(PDF)

Figure S3 Genotyping error check. 2D-cluster plots for the representative SNPs obtained from chromosome 9 (A), chromosome 1 (B), chromosome 5 (C), and chromosome 12 (D) that showed genome-wide significance. These 2D cluster plots were drawn by Genotyping Console 4.1 software (Affymetrix).
(PDF)

Figure S4 GWAS results of two subtypes. Association results of the Present GWAS for the two subtypes of POAG, HPG (A) and NPG (B). The horizontal dashed line in each plot indicates the Bonferroni correction threshold for each study.
(PDF)

Figure S5 Evaluation of previously reported loci/genes. Evaluation of the POAG-associated loci/genes reported previously using our Present GWAS data. The genes located in the loci are as the follows: (A) ZP4, (B) PLXDC2, (C) TMTC2, (D) SRBD1, (E) ELOVL5, (F) CAV1/CAV2, and (G) TMCO1. Each locus was evaluated by the results of POAG vs control, POAG/HPG vs control, and POAG/NPG vs control. The plotted SNPs were selected from QC filtered SNPs. Target genes are placed in the center of the 500-kb spanned region. Plots are shown with genomic annotation and HapMap LD (JPT+CHB) made by the UCSC Genome Browser (Human Mar. 2006).
(PDF)

Figure S6 Population stratification analysis. Population stratification analysis by EIGENSTRAT in the Present GWAS data set. POAG samples separated with HPG and NPG groups were applied. The version of HapMap reference data is release22 (Build36). Since Control, NPG, HPG, and HapMap JPT samples were tightly overlapped, only the plots for NPG (yellow cross) are visible.
(PDF)

Table S1 Genome-wide significant SNPs that passed the Bonferroni correction threshold in the Present GWAS.
(PDF)

Table S2 Analysis of confounding effects of age and sex for the candidate SNPs.
(PDF)

Table S3 Present GWAS results in 9p21.3 locus.
(PDF)

Table S4 Combined GWAS results in 9p21.3 locus.
(PDF)

Table S5 Association results of Present GWAS for previously reported SNPs.
(PDF)

Table S6 Characteristics of the samples.
(PDF)

Supporting Information S1 Quality control for genotyping.
(PDF)

Acknowledgments

The authors wish to thank all the patients and volunteers who enrolled in the study. We also thank Professor T. Miki for managing the anonymous code-assignment process; M. Yamashita, S. Ohashi, and N. Saito for processing blood samples and performing genotyping; H. Yamada for the assistance in clinical information analysis; R. Sato and F. Sato (SASA Plus Co., Ltd., Fukuoka, Japan) for the management of genotype data and building the analyzing system; T. Ichikawa for excellent secretarial assistance; and J. Bush for reviewing the manuscript.

Author Contributions

Conceived and designed the experiments: SK KT. Performed the experiments: MN YI NO MU KI HA KM. Analyzed the data: MN YT SK KT. Contributed reagents/materials/analysis tools: YI MF MU KI MK KM SK. Wrote the paper: MN YI YT KM SK KT.

References

1. Quigley HA, Broman AT (2006) The number of people with glaucoma worldwide in 2010 and 2020. Br J Ophthalmol 90: 262–267.
2. Kwon YH, Fingert JH, Kuehn MH, Alward WL (2009) Primary open-angle glaucoma. N Engl J Med 360: 1113–1124.
3. European Glaucoma Society (2008) Terminology and guidelines for glaucoma, 3rd edition (Editrice Dogma, Savona, Italy).
4. Iwase A, Suzuki Y, Araie M, Yamamoto T, Abe H, et al. (2004) The prevalence of primary open-angle glaucoma in Japanese: the Tajimi Study. Ophthalmology 111: 1641–1648.
5. Klein BE, Klein R, Sponsel WE, Franke T, Cantor LB, et al. (1992) Prevalence of glaucoma. The Beaver Dam Eye Study. Ophthalmology 99: 1499–1504.
6. Heijl A, Leske MC, Bengtsson B, Hyman L, Bengtsson B, et al. (2002) Reduction of intraocular pressure and glaucoma progression: results from the Early Manifest Glaucoma Trial. Arch Ophthalmol 120: 1268–1279.
7. Leskea MC, Heijl A, Hyman L, Bengtsson B, Komaroff E (2004) Factors for progression and glaucoma treatment: the Early Manifest Glaucoma Trial. Curr Opin Ophthalmol 15: 102–106.
8. Hewitt AW, Craig JE, Mackey DA (2006) Complex genetics of complex traits: the case of primary open-angle glaucoma. Clin Experiment Ophthalmol 34: 472–484.
9. Fan BJ, Wiggs JL (2010) Glaucoma: genes, phenotypes, and new directions for therapy. J Clin Invest 120: 3064–3072.
10. Nakano M, Ikeda Y, Taniguchi T, Yagi T, Fuwa M, et al. (2009) Three susceptible loci associated with primary open-angle glaucoma identified by genome-wide association study in a Japanese population. Proc Natl Acad Sci U S A 106: 12838–12842.
11. Jiao X, Yang Z, Yang X, Chen Y, Tong Z, et al. (2009) Common variants on chromosome 2 and risk of primary open-angle glaucoma in the Afro-Caribbean population of Barbados. Proc Natl Acad Sci U S A 106: 17105–17110.
12. Meguro A, Inoko H, Ota M, Mizuki N, Bahram S (2010) Genome-wide association study of normal tension glaucoma: common variants in SRBD1 and ELOVL5 contribute to disease susceptibility. Ophthalmology 117: 1331–1338 e1335.
13. Thorleifsson G, Walters GB, Hewitt AW, Masson G, Helgason A, et al. (2010) Common variants near CAV1 and CAV2 are associated with primary open-angle glaucoma. Nat Genet 42: 906–909.
14. Burdon KP, Macgregor S, Hewitt AW, Sharma S, Chidlow G, et al. (2011) Genome-wide association study identifies susceptibility loci for open angle glaucoma at TMCO1 and CDKN2B-AS1. Nat Genet 43: 574–578.
15. Kuehn MH, Wang K, Roos B, Stone EM, Kwon YH, et al. (2011) Chromosome 7q31 POAG locus: ocular expression of caveolins and lack of association with POAG in a US cohort. Mol Vis 17: 430–435.

16. Rao KN, Kaur I, Chakrabarti S (2009) Lack of association of three primary open-angle glaucoma-susceptible loci with primary glaucomas in an Indian population. Proc Natl Acad Sci U S A 106: E125–126; author reply E127.
17. Ramdas WD, van Koolwijk LM, Lemij HG, Pasutto F, Cree AJ, et al. (2011) Common genetic variants associated with open-angle glaucoma. Hum Mol Genet 20: 2464–2471.
18. Japan Glaucoma Society (2006) Guidelines for glaucoma, 2nd edition.
19. Mantel N, Haenszel W (1959) Statistical aspects of the analysis of data from retrospective studies of disease. J Natl Cancer Inst 22: 719–748.
20. McPherson R, Pertsemlidis A, Kavaslar N, Stewart A, Roberts R, et al. (2007) A common allele on chromosome 9 associated with coronary heart disease. Science 316: 1488–1491.
21. Helgadottir A, Thorleifsson G, Manolescu A, Gretarsdottir S, Blondal T, et al. (2007) A common variant on chromosome 9p21 affects the risk of myocardial infarction. Science 316: 1491–1493.
22. Samani NJ, Erdmann J, Hall AS, Hengstenberg C, Mangino M, et al. (2007) Genomewide association analysis of coronary artery disease. N Engl J Med 357: 443–453.
23. Wellcome Trust Case Control Consortium (2007) Genome-wide association study of 14,000 cases of seven common diseases and 3,000 shared controls. Nature 447: 661–678.
24. Scott LJ, Mohlke KL, Bonnycastle LL, Willer CJ, Li Y, et al. (2007) A genome-wide association study of type 2 diabetes in Finns detects multiple susceptibility variants. Science 316: 1341–1345.
25. Saxena R, Voight BF, Lyssenko V, Burtt NP, de Bakker PI, et al. (2007) Genome-wide association analysis identifies loci for type 2 diabetes and triglyceride levels. Science 316: 1331–1336.
26. Zeggini E, Scott LJ, Saxena R, Voight BF, Marchini JL, et al. (2008) Meta-analysis of genome-wide association data and large-scale replication identifies additional susceptibility loci for type 2 diabetes. Nat Genet 40: 638–645.
27. Harismendy O, Notani D, Song X, Rahim NG, Tanasa B, et al. (2011) 9p21 DNA variants associated with coronary artery disease impair interferon-gamma signalling response. Nature 470: 264–268.
28. Ramdas WD, van Koolwijk LM, Ikram MK, Jansonius NM, de Jong PT, et al. (2010) A genome-wide association study of optic disc parameters. PLoS Genet 6: e1000978.
29. Traggiai E, Becker S, Subbarao K, Kolesnikova L, Uematsu Y, et al. (2004) An efficient method to make human monoclonal antibodies from memory B cells: potent neutralization of SARS coronavirus. Nat Med 10: 871–875.
30. Ueta M, Sotozono C, Nakano M, Taniguchi T, Yagi T, et al. (2010) Association between prostaglandin E receptor 3 polymorphisms and Stevens-Johnson syndrome identified by means of a genome-wide association study. J Allergy Clin Immunol 126: 1218–1225 e1210.
31. Frazer KA, Ballinger DG, Cox DR, Hinds DA, Stuve LL, et al. (2007) A second generation human haplotype map of over 3.1 million SNPs. Nature 449: 851–861.

in patients with psoriasis, in order to carry out a subgroup analysis.

The present findings suggest that high serum CRH level, possibly in response to stress, stimulates skin mast cells to release VEGF and contribute to skin inflammation evident in patients with severe psoriasis. Continuous or repeated stimulation may lead to decreased expression of skin CRHR-1, as we showed recently with cultured mast cells,[9] and hence decreased VEGF, as was evident in patients with mild disease. CRH and CRHR-1 may therefore participate in the pathogenesis of psoriasis and AD, especially when worsened with stress, through mast-cell activation to release VEGF. Mast-cell blockers may provide novel treatment approaches.

We thank Dr C. D. Spielberger (University of South Florida, Tampa, Fla) for assistance with his STAI, as well as Dr James Marchand (Tufts University) and Duraisamy Kempuraj (University of Iowa) for assistance with the immunohistochemistry.

Magdalini Vasiadi, BSc[a,b,c]
Anastasia Therianou, MD[d]
Kyriaki Sideri, MD[c]
Marilena Smyrnioti, BSc, MA[c]
Nikolaos Sismanopoulos, MD[a,c]
Danae A. Delivanis, MD[a,l]
Shahrzad Asadi, PharmD[a,f]
Alexandra Katsarou-Katsari, MD, PhD[d]
Theodora Petrakopoulou, MD[g]
Athanasios Theoharides, MD, PhD[h]
Christina Antoniou, MD, PhD[d]
Evaggelia Papadavid, MD, PhD[i]
Nikolaos Stavrianeas, MD, PhD[i]
Dimitrios Kalogeromitros, MD, PhD[c]†
Theoharis C. Theoharides, MS, PhD, MD[a,b,c,j,k]

From [a]the Molecular Immunopharmacology and Drug Discovery Laboratory, Department of Molecular Physiology and Pharmacology, and [j]the Department of Biochemistry, Tufts University School of Medicine, Boston, Mass; [b]the Sackler School of Graduate Biomedical Sciences, Tufts University, Boston, Mass; [c]the Allergy Clinical Research Center, [e]the Pain Relief Clinic, Second Department of Anesthesiology, and [l]the Second Department of Dermatology, Attikon Hospital, Athens University Medical School, Athens, Greece; [d]the First Department of Dermatology, A. Sygros Hospital, Athens University Medical School, Athens, Greece; [f]the Department of Pharmacy, Tufts Medical Center, Tufts University School of Medicine, Boston, Mass; [g]the Oncology Hospital, IKA, Athens, Greece; [h]the Ano Toumba Polyclinic, IKA, Thessaloniki, Greece; [k]the Department of Internal Medicine, Tufts University School of Medicine and Tufts Medical Center, Boston, Mass; and [i]the Department of Internal Medicine, University of Connecticut Medical Center, Hartford, Conn. E-mail: theoharis.theoharides@tufts.edu.

†Deceased.

This work was supported in part by the National Institutes of Health grant AR47652 awarded to T.C.T.

Disclosure of potential conflict of interest: The authors declare that they have no relevant conflicts of interest.

REFERENCES

1. Guttman-Yassky E, Nograles KE, Krueger JG. Contrasting pathogenesis of atopic dermatitis and psoriasis, part I: clinical and pathologic concepts. J Allergy Clin Immunol 2011;127:1110-8.
2. Metz M, Grimbaldeston MA, Nakae S, Piliponsky AM, Tsai M, Galli SJ. Mast cells in the promotion and limitation of chronic inflammation. Immunol Rev 2007;217: 304-28.
3. Theoharides TC, Cochrane DE. Critical role of mast cells in inflammatory diseases and the effect of acute stress. J Neuroimmunol 2004;146:1-12.
4. Theoharides TC, Singh LK, Boucher W, Pang X, Letourneau R, Webster E, et al. Corticotropin-releasing hormone induces skin mast cell degranulation and increased vascular permeability, a possible explanation for its pro-inflammatory effects. Endocrinology 1998;139:403-13.
5. Crompton R, Clifton VL, Bisits AT, Read MA, Smith R, Wright IM. Corticotropin-releasing hormone causes vasodilation in human skin via mast cell-dependent pathways. J Clin Endocrinol Metab 2003;88:5427-32.
6. Slominski A, Wortsman J. Neuroendocrinology of the skin. Endocr Rev 2000;21: 457-87.
7. Slominski A. On the role of the corticotropin-releasing hormone signalling system in the aetiology of inflammatory skin disorders. Br J Dermatol 2009;160:229-32.
8. Fountoulakis KN, Papadopoulou M, Kleanthous S, Papadopoulou A, Bizeli V, Nimatoudis I, et al. Reliability and psychometric properties of the Greek translation of the State-Trait Anxiety Inventory form Y: preliminary data. Ann Gen Psychiatry 2006;5:2.
9. Asadi S, Alysandratos KD, Angelidou A, Miniati A, Sismanopoulos N, Vasiadi M, et al. Substance P (SP) induces expression of functional corticotropin-releasing hormone receptor-1 (CRHR-1) in human mast cells. J Invest Dermatol 2012;132:324-9.

Available online February 22, 2012.
doi:10.1016/j.jaci.2012.01.041

Epistatic interaction between Toll-like receptor 3 (*TLR3*) and prostaglandin E receptor 3 (*PTGER3*) genes

To the Editor:

We previously reported that conjunctival eosinophilic infiltration in murine experimental allergic conjunctivitis (EAC) was significantly less marked in Toll-like receptor 3 gene (*TLR3*) knockout (KO) mice[1] and significantly more marked in prostaglandin E receptor 3 (EP3) gene (*PTGER3*) KO mice than in wild-type mice.[2] Considering the opposite roles of TLR3 and EP3 in allergic conjunctivitis, we speculate the possibility of unknown functional interaction between TLR3 and EP3.

Intriguingly, we have also reported that Stevens-Johnson syndrome (SJS)/toxic epidermal necrolysis (TEN) accompanied by severe ocular surface complications was associated with *TLR3* gene polymorphisms[3] and *PTGER3* polymorphisms.[4] SJS is an acute inflammatory vesiculobullous reaction of the skin and mucosa, often including the ocular surface,[5] and TEN occurs with its progression. SJS/TEN with ocular surface complications often results in severe and definitive sequelae, such as vision loss (see Fig E1 in this article's Online Repository at www.jacionline.org).[6]

For the past decade, single nucleotide polymorphisms (SNPs) have been widely used as genetic markers for identifying human disease-susceptibility genes. However, it has become apparent that gene-gene interactions should be considered in addition to major single-locus effects.[7] In particular, nonadditive (epistatic) models for some complex diseases fit to actual observations, suggesting interactions involving multiple loci.

In this study we examined whether there are functional interaction between TLR3 and EP3. Moreover, we also examined whether there is an epistatic interaction between *TLR3* and *PTGER3* polymorphisms in patients with SJS/TEN with ocular surface complications.

This study was approved by the institutional review board of Kyoto Prefectural University of Medicine and the University of Tokyo, Graduate School of Medicine. All experimental procedures were conducted in accordance with the principles of the Helsinki Declaration. Details of the patients and methods are described in the Methods section in this article's Online Repository at www.jacionline.org. The primers and probes used in this study are shown in Table E1 in this article's Online Repository at www.jacionline.org.

First, we examined the functional interaction between TLR3 and EP3 by using *TLR3* KO, *PTGER3* KO, and *TLR3/PTGER3* double-knockout (DKO) mice in addition to our EAC model.

We compared conjunctival eosinophil infiltration in wild-type, *TLR3* KO, *PTGER3* KO, and *TLR3/PTGER3* DKO mice. Although sensitization (intracutaneous and intraperitoneal injection of short ragweed pollen [RW; Polysciences, Inc, Warrington, Pa] adsorbed on aluminum hydroxide [200 μg of RW and 2.6 mg of alum]) without challenge (RW eye drop) did not affect the number of eosinophils after sensitization and challenge, the number of eosinophils in the lamina propria mucosae of the conjunctiva was significantly increased in all of them compared with those in PBS-challenged control animals, and the number after sensitization and challenge in *PTGER3* KO mice was significantly larger and significantly lower in *TLR3* KO than in wild-type mice, as we have reported previously.[1,2] Because TLR3 could regulate allergic inflammation in the absence of exogenous viral infection or the TLR3 ligand, it is possible that in our allergic conjunctivitis model endogenous RNA from tissues or cells stimulates TLR3.[1] With respect to EP3, one of the prostaglandin E receptors (EP1-EP4), our earlier observations suggested that during the elicitation phase of our EAC model, prostaglandin E_2 is synthesized in the conjunctival epithelium through microsomal prostaglandin E synthase 1.[2]

Furthermore, in *TLR3/PTGER3* DKO mice the number of eosinophils in the lamina propria mucosae of the conjunctiva was decreased to a level similar to the number of eosinophils in the lamina propria mucosae of the conjunctiva in *TLR3* KO mice and was significantly lower than the number of eosinophils in the lamina propria mucosae of the conjunctiva in not only *PTGER3* KO mice but also in wild-type mice (Fig 1). In addition, we previously reported that in human conjunctival epithelial cells the EP3 agonist suppressed the production of cytokines, such as thymic stromal lymphopoietin[8] and RANTES,[9] induced by polyinosinic:polycytidylic acid, a TLR3 ligand. Thymic stromal lymphopoietin and RANTES play important roles in the recruitment of eosinophils. These results suggest that EP3 negatively regulates the eosinophilic infiltration of EAC induced by TLR3, which causes reduced eosinophilic conjunctival inflammation in *TLR3/PTGER3* DKO mice, despite the pronounced eosinophilic conjunctival inflammation seen in *PTGER3* KO mice.

We have reported that the frequency of carriers of the HLA-A*0206 allele is significantly higher among Japanese patients with severe ocular surface complications.[10] We have also performed SNP association analysis of candidate genes and documented the associated polymorphisms of several immune-related genes, including *TLR3*,[3] IL-4 receptor *(IL4R)*,[11] *IL13*, and Fas ligand *(FasL)* in Japanese patients with SJS/TEN. Furthermore, we have performed a genome-wide association study of the patients with SJS/TEN and found associations between 6 SNPs in the *PTGER3* gene and the Japanese patients with SJS/TEN.[4]

We carried out a statistical search for interactions between all possible pairs of loci by applying high-dimensional variable selection methods, such as Sure Independence Screening (SIS) and LASSO, to the comprehensive dataset obtained from our previous studies for a total of 14 immune-related genes (see Table E2 in this article's Online Repository at www.jacionline.org), including *PTGER3* and *TLR3*. After filtering with the standard SNP quality control filter, 36 SNPs were used for SIS to scan a total of 5778 ($3 \times 36 + 9 \times 36 \times [36\text{-}1]/2$) dummy variables. As a result, iterative SIS reported 2 variables with susceptible effects on SJS, which were involved in locus pairs of *PTGER3-TLR3* and *HLA-A-IL1A*, respectively (see Table E3 in this article's Online Repository at www.jacionline.org). The result showed that the *PTGER3* rs.4147114G/C SNP with the *TLR3* rs.3775296T/T SNP exhibited a higher odds ratio (OR, 25.3; $P = .0000527$) than only the *PTGER3* rs.4147114G/C SNP (OR, 2.66; $P = .0023$) or only the *TLR3* rs.3775296T/T SNP (OR, 5.35; $P = .00025$). These 2 susceptible interactions were also confirmed by using LASSO.

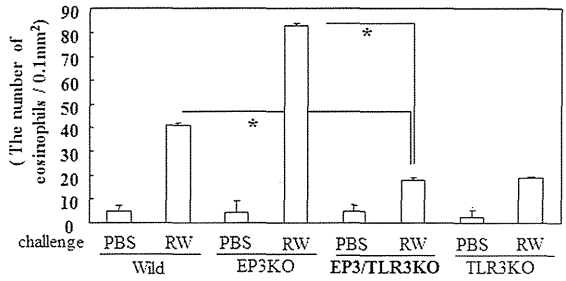

FIG 1. Functional interaction between EP3 and TLR3. In *TLR3/PTGER3* DKO mice the number of eosinophils in the lamina propria mucosae of the conjunctiva was decreased to a level similar to that seen in *TLR3* KO mice and was significantly lower than that seen in either *PTGER3* KO or wild-type mice. Data are shown as means ± SEMs of samples from all the mice examined (wild-type: phosphate-buffered saline, n = 24; RW, n = 28; *PTGER3* KO mice: phosphate-buffered saline, n = 23; RW, n = 25; EP3/TLR3 DKO mice: phosphate-buffered saline, n = 4; RW, n = 11; *TLR3* KO mice: phosphate-buffered saline, n = 12; RW, n = 12). *$P < .0005$.

Next, we focused on the epistatic interaction between *TLR3* and *PTGER3* and analyzed the additional 10 SNPs of *TLR3* and 32 SNPs of *PTGER3*, resulting in a total of 17 SNPs of *TLR3* and 38 SNPs of *PTGER3*. All genotyping results agreed with Hardy-Weinberg equilibrium ($P > .01$) in both the case and control samples. These results showed that 5 additional SNPs of *TLR3* and 14 SNPs of *PTGER3*, a total of 7 SNPs of *TLR3* and 20 SNPs of *PTGER3*, were associated with SJS/TEN with ocular complications in addition to the previously reported 2 SNPs of *TLR3* and 6 SNPs of *PTGER3* (see Tables E4 and E5 in this article's Online Repository at www.jacionline.org). Moreover, we investigated linkage disequilibrium (LD) in *TLR3* and *PTGER3* regions by using the squared correlation coefficient (1 SNP of *TLR3* [rs3775293] for which the minor allele frequency in both cases and control subjects was less than 5% was excluded) and identified 3 solid-spine LD blocks in each region. Iterative SIS reported 14 variables with nonzero regression coefficients as if connecting the 5′ region of *TLR3* (block 1) and the 3′ region of *PTGER3* (block 1, Fig 2).

We previously reported that the expression of EP3, the protein of the *PTGER3* gene, was downregulated in the conjunctival epithelium of patients with SJS/TEN with ocular surface complications.[4,12]

Although *TLR3* mRNA expression might also be downregulated in patients with SJS/TEN (see Fig E2 in this article's Online Repository at www.jacionline.org), our immunohistologic analysis did not clearly detect downregulation of the protein (see Fig E3 in this article's Online Repository at www.jacionline.org).

In the conjunctival epithelium of patients with SJS/TEN, EP3 was remarkably downregulated, and TLR3 might also be downregulated. Because EP3 might be more strongly downregulated than TLR3 in these patients, it is possible that EP3 is incapable of preventing TLR3-associated inflammation in patients with SJS/TEN.

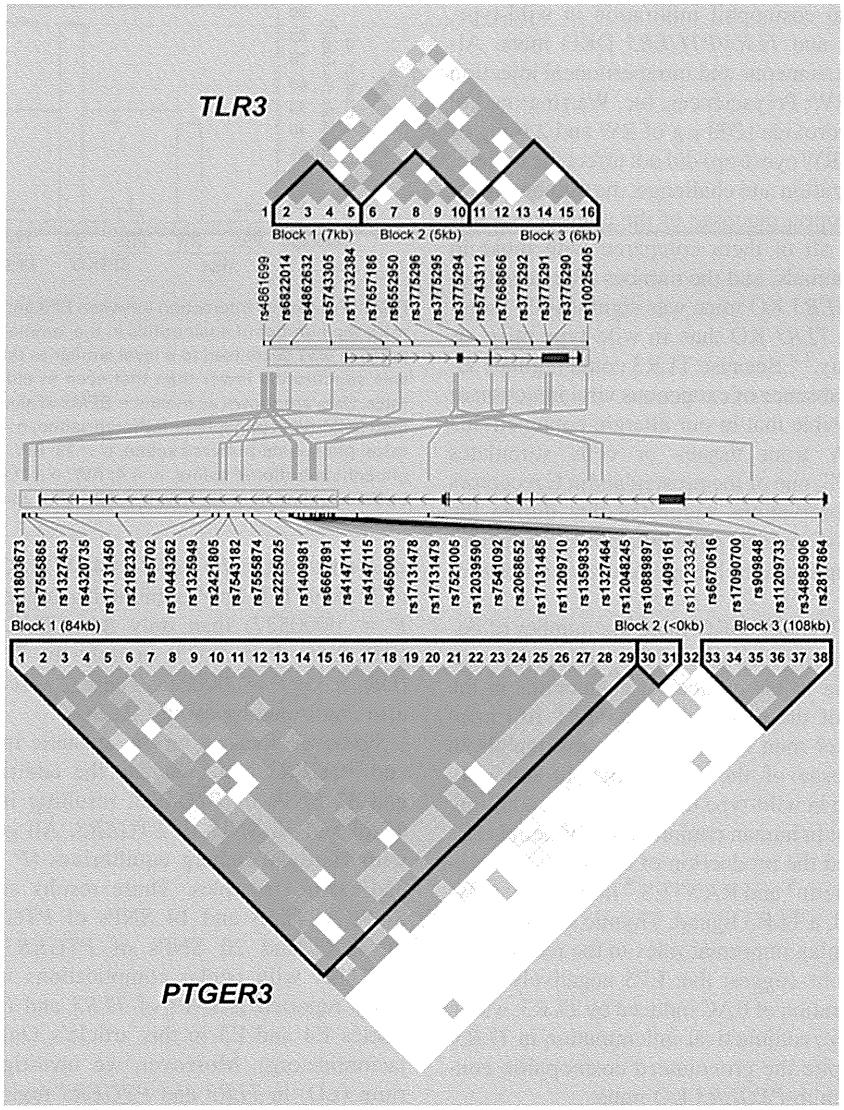

FIG 2. LD in EP3 and TLR3 regions. LD in the *TLR3* and *PTGER3* regions show 3 solid-spine LD blocks in each region. Iterative SIS reported 14 variables with nonzero regression coefficients, as if connecting the 5′ region of *TLR3* and the 3′ region of *PTGER3*.

In conclusion, we have suggested the functional interaction between TLR3 and EP3 supported by their epistatic interaction that confers an increased risk for SJS with severe ocular surface complications.

Mayumi Ueta, MD, PhD[a,b]
Gen Tamiya, PhD[c]
Katsushi Tokunaga, PhD[d]
Chie Sotozono, MD, PhD[a]
Masao Ueki, PhD[c]
Hiromi Sawai, PhD[d]
Tsutomu Inatomi, MD, PhD[a]
Toshiyuki Matsuoka, MD, PhD[e]
Shizuo Akira, MD, PhD[f]
Shuh Narumiya, MD, PhD[h]
Kei Tashiro, MD, PhD[g]
Shigeru Kinoshita, MD, PhD[a]

From the Departments of [a]Ophthalmology and [g]Genomic Medical Sciences, Kyoto Prefectural University of Medicine, Kyoto, Japan; [b]the Research Center for Inflammation and Regenerative Medicine, Faculty of Life and Medical Sciences, Doshisha University, Kyoto, Japan; [c]the Advanced Molecular Epidemiology Research Institute, Faculty of Medcine, Yamagata University, Yamagata, Japan; [d]the Department of Human Genetics, Graduate School of Medicine, University of Tokyo, Tokyo, Japan; [e]Tenri Yorozu Hospital, Nara, Japan; [f]the Department of Host Defense, Research Institute for Microbial Diseases, Osaka University, Osaka, Japan; and [h]the Department of Pharmacology and Faculty of Medicine, Kyoto University, Kyoto, Japan. E-mail: mueta@koto.kpu-m.ac.jp.

Supported in part by grants-in-aid for scientific research from the Japanese Ministry of Health, Labour and Welfare, the Japanese Ministry of Education, Culture, Sports, Science and Technology; a research grant from the Kyoto Foundation for the Promotion of Medical Science; and the Intramural Research Fund of Kyoto Prefectural University of Medicine.

Disclosure of potential conflict of interest: S. Narumiya has received research support from One Pharmaceuticals Co Ltd. The rest of the authors declare they have no relevant conflicts of interest.

REFERENCES

1. Ueta M, Uematsu S, Akira S, Kinoshita S. Toll-like receptor 3 enhances late-phase reaction of experimental allergic conjunctivitis. J Allergy Clin Immunol 2009;123: 1187-9.